AGU PUBLICATIONS

JGR

Journal of Geophysical Research: Earth Surface

RESEARCH ARTICLE
10.1002/2015JF003525

**Key Points:**
- There is an optimum debris flow composition for maximum runout
- Debris flow runout depends at least as much on composition as on topography
- Deposit geometry is largely controlled by debris flow composition

**Supporting Information:**
- Readme
- Table S1
- Movie S1
- Movie S2
- Movie S3
- Movie S4
- Movie S5
- Movie S6
- Movie S7
- Movie S8

**Correspondence to:**
T. de Haas,
T.deHaas@uu.nl

**Citation:**
de Haas, T., L. Braat, J. R. F. W. Leuven, I. R. Lokhorst, and M. G. Kleinhans (2015), Effects of debris flow composition on runout, depositional mechanisms, and deposit morphology in laboratory experiments, *J. Geophys. Res. Earth Surf.*, *120*, 1949–1972, doi:10.1002/2015JF003525.

Received 2 MAR 2015
Accepted 31 AUG 2015
Accepted article online 5 SEP 2015
Published online 30 SEP 2015



# Effects of debris flow composition on runout, depositional mechanisms, and deposit morphology in laboratory experiments

**Tjalling de Haas[1], Lisanne Braat[1], Jasper R. F. W. Leuven[1], Ivar R. Lokhorst[1], and Maarten G. Kleinhans[1]**

[1] Faculty of Geosciences, Universiteit Utrecht, Utrecht, Netherlands

**Abstract** Predicting debris flow runout is of major importance for hazard mitigation. Apart from topography and volume, runout distance and area depends on debris flow composition and rheology, but how is poorly understood. We experimentally investigated effects of composition on debris flow runout, depositional mechanisms, and deposit geometry. The small-scale experimental debris flows were largely similar to natural debris flows in terms of flow behavior, deposit morphology, grain size sorting, channel width-depth ratio, and runout. Deposit geometry (lobe thickness and width) in our experimental debris flows is largely determined by composition, while the effects of initial conditions of topography (i.e., outflow plain slope and channel slope and width) and volume are negligible. We find a clear optimum in the relations of runout with coarse-material fraction and clay fraction. Increasing coarse-material concentration leads to larger runout. However, excess coarse material results in a large accumulation of coarse debris at the flow front and enhances diffusivity, increasing frontal friction and decreasing runout. Increasing clay content initially enhances runout, but too much clay leads to very viscous flows, reducing runout. Runout increases with channel slope and width, outflow plain slope, debris flow volume, and water fraction. These results imply that debris flow runout depends at least as much on composition as on topography. This study improves understanding of the effects of debris flow composition on runout and may aid future debris flow hazard assessments.

## 1. Introduction

Debris flows are common phenomena in mountainous regions. They differ from rock avalanches and sediment-laden water floods because both solid and fluid forces influence their motion and govern their rheological properties [*Costa*, 1988; *Iverson*, 1997]. Typically, debris flows contain 20% to 60% water by volume [*Costa*, 1988; *Pierson*, 2005], peak velocities can surpass 10 m/s, and large flows can exceed 1 $km^3$ [e.g., *Iverson*, 1997]. They denude mountainsides, inundate channels, floodplains, and alluvial fans, and thereby present a major hazard for people and structures [e.g., *Jakob*, 2005]. The socioeconomic impacts of debris flows may grow with the current increase of landscape exploitation and extreme precipitation events and permafrost degradation forced by global warming [e.g., *Rebetez et al.*, 1997; *Jakob and Friele*, 2010; *Stoffel et al.*, 2014].

The assessment of runout distance and area is critical for delineating areas at risk from debris flows [*D'Agostino et al.*, 2010]. Several methods have been proposed to predict debris flow runout [e.g., *Rickenmann*, 2005; *D'Agostino et al.*, 2010; *Griswold and Iverson*, 2008; *Scheidl et al.*, 2013]. These methods depend mainly on topography (i.e., the slope, width, and length of the upstream channel and the slope of the outflow plain) and debris flow volume [e.g., *Takahashi*, 1991; *Bathurst et al.*, 1997; *Rickenmann*, 1999; *Berti and Simoni*, 2007]. However, debris flow composition has often been neglected for practical reasons, although it has a profound effect on debris flow dynamics and runout distance [e.g., *Whipple and Dunne*, 1992; *Scheidl and Rickenmann*, 2010; *Hürlimann et al.*, 2015].

Debris flow composition is commonly neglected because it is very difficult to constrain material properties from debris flow deposits in the field [e.g., *Iverson et al.*, 2010]. Natural debris flows are monitored in a few high-frequency debris flow torrents [e.g., *Hürlimann et al.*, 2003; *Takahashi*, 2009; *Zhou and Ng*, 2010; *McCoy et al.*, 2010; *Marchi and Tecca*, 2013], but monitoring faces many difficulties because of the rapid, short-lasting, infrequent, and destructive nature of debris flows. Debris flows cause the greatest threat when they move

across unconfined slopes of alluvial fans, which may be densely populated [*Cavalli and Marchi*, 2008]. However, they are generally not actively monitored on such sites.

Debris flow composition strongly affects deposit geometry, such as the height and width of levees and lobes [e.g., *Whipple and Dunne*, 1992; *Coussot et al.*, 1998; *Major and Iverson*, 1999]. However, the relation between debris flow composition and deposit geometry (i.e., lobe and levee thickness and width) is still poorly understood.

We use experiments to investigate the effects of debris flow composition on runout distance and deposit geometry. Several authors have previously used laboratory flumes to simulate debris flows [e.g., *Van Steijn and Coutard*, 1989; *Liu*, 1996; *Major and Iverson*, 1999; *D'Agostino et al.*, 2010; *Hürlimann et al.*, 2015]. Well-developed unchanneled experimental debris flows with self-formed levees and a marked depositional lobe have only been produced in the large-scale U.S. Geological Survey (USGS) laboratory flume [e.g., *Iverson et al.*, 2010] but not in smaller-scale flumes. Small-scale experiments are useful because they allow experiments to be done in large numbers and for a wide range of compositions. *Iverson and Denlinger* [2001] and *Iverson et al.* [2010] suggested that dynamic similarity between natural and small-scale debris flows is probably unattainable, as small-scale debris flows are likely to show disproportionately large effects of yield strength, viscous flow resistance, and grain inertia, while showing a disproportionately small effect of pore fluid pressure. Nonetheless, despite these scale effects, we managed to create small experimental debris flows that show similar flow behavior, grain segregation, runout, and deposit morphology as natural debris flows [e.g., *Blair*, 1999; *Johnson et al.*, 2012].

Here we experimentally investigate effects of debris flow composition on debris flow runout distance and area, depositional mechanisms, and deposit geometry. This paper is structured as follows. We first detail layout and boundary conditions of the experimental flume and laboratory experiments. Then we detail measurement techniques and dimensionless parameters used to evaluate flow regimes in the experimental debris flows and to address scaling. We present observations of the morphology and sediment sorting and infer flow regimes and effects of debris flow composition, volume, and topography on runout distance and deposit morphology. Finally, we discuss effects of debris flow composition on depositional mechanisms, runout distance, and deposit geometry and elaborate on the scaling of debris flows in small-scale laboratory flumes.

## 2. Methods

### 2.1. Methodology

We conducted a series of small-scale debris flow experiments with systematic variations of angular gravel (2–5 mm), clay (kaolinite), and water fractions relative to a reference debris flow mixture, consisting of gravel, sand, and clay mixed with water (Tables 1 and S1 in the supporting information). The gravel and clay fractions are defined as the fraction within the total solids volume, and the water fraction is defined as the volume of water relative to the total debris flow volume (solids and water). For simplicity, we converted mass to volume by assuming a constant solids density of 2650 kg/m$^3$, which might introduce a small volume underestimation for the debris flows rich in basaltic gravel (basalt density ≈3400 kg/m$^3$; underestimation ∼2% for most debris flows and up to 9% for the most gravel-rich debris flow). We also tested the topographic effects of channel width, channel length, channel slope, and outflow plain slope. Finally, the effect of outflow plain composition was tested, by using an initial unconsolidated ∼1 cm thick bed of sand, a fixed rough bed (sand glued to a plate), and a fixed smooth bed (plastic). After initial tests we selected a reference sediment mixture (see section 2.3) for all experiments and gravel, clay, and water fractions were systematically varied relative to this mixture. We found that experiments were repeatable, although natural variability caused considerable variations in some debris flows. To account for the effects of natural variability, we generally conducted each experimental setting at least 3 times. Using photograph, video, and digital elevation model (DEM) analyses, we mapped the dynamics, morphology, and sediment sorting of the debris flows. This data documented flow velocity and flow depth of the debris flows during motion and the runout distance and area, lobe width, lobe height, and levee height of deposits.

### 2.2. Experimental Setup and Data Collection

The experimental flume consisted of a straight, rectangular, channel of 2 m long and 12 cm wide (Figure 1), connected to an unconstrained lower angle outflow plain. Upstream, the channel was connected to a manual mixing tank with a gate that opened electromagnetically for rapid release of well-mixed debris. Sediment and water were agitated in the mixing tank for ∼20 s, and agitation stopped simultaneously with gate opening.

**Table 1.** Varied Debris Flow Composition and Topographic Parameters[a]

| Parameter | Unit | Reference | Range | Number of Experiments |
|---|---|---|---|---|
| *Debris Flow Composition* | | | | |
| Gravel fraction | g | 900 | 0–3624 | 47 |
| | vol % | 18 | 0–72 | |
| | wt % | 14 | 0–56 | |
| Clay fraction | g | 100 | 0–1899 | 50 |
| | vol % | 2.0 | 0–38 | |
| | wt % | 1.5 | 0–29 | |
| Water fraction | g | 1500 | 1200–2500 | 33 |
| | vol % | 44 | 39–57 | |
| | wt % | 23 | 19–33 | |
| Total mass[b] | g | 6500 | 1950–11050 | 27 |
| Total volume[b] | $m^3$ | 0.0034 | 0.0010–0.0058 | 27 |
| *Topography* | | | | |
| Channel slope | deg | 30 | 22–34 | 41 |
| Outflow plain slope | deg | 10 | 0–15 | 29 |
| Channel width | cm | 12 | 4.5–12 | 16 |
| Channel length | m | 2 | 2–3 | 16 |

[a]Note that the bulk of the debris flow mixture consisted of sand, but this was not systematically varied and therefore not shown in this table.
[b]Similar series.

The gate opened by swinging upward. Relatively soft tap water was used in the experiments (5.4° DH). To simulate natural bed roughness, the channel bed and sidewalls were covered with sandpaper (grade 80), whereas the outflow plain was covered by a layer of ~1 cm unconsolidated reference mixture (without water and clay).

In the channel floor a hatch was present 76 cm upstream of the intersection point of channel and outflow plain. This hatch was opened at a constant time interval (1.5 s) after release of debris from the mixing tank, to divert the debris flow tail and prevent it from filling the initial channel and obscuring sorting patterns. A similar approach was followed in debris flow experiments in the USGS flume by *Johnson et al.* [2012]. Truncation of the tail did not affect runout or lobe thickness as the dilute tail mainly backfilled the channel in between the levees. The estimated volume of the truncated tail is 10–20% of the total volume at maximum.

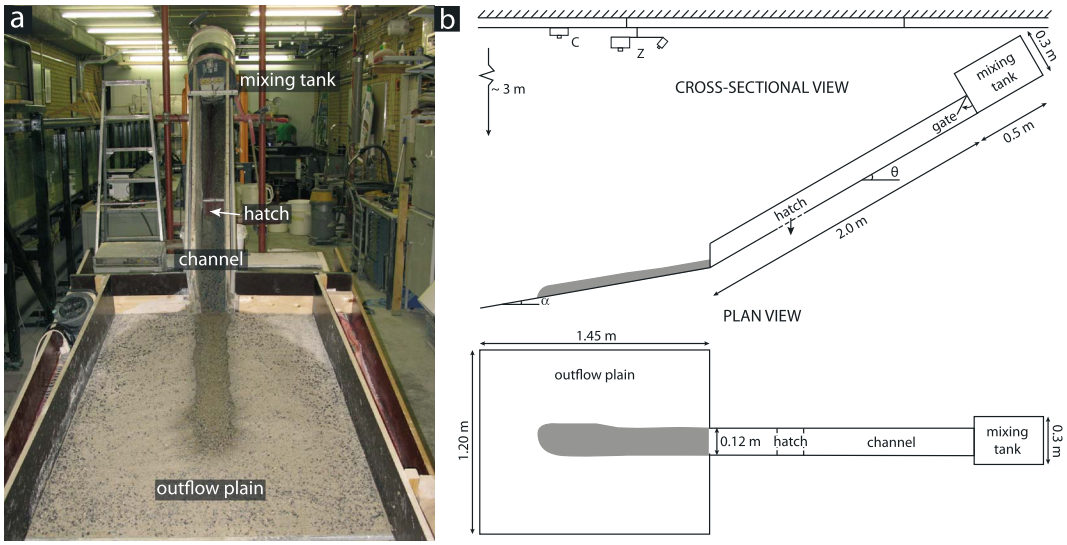


**Figure 1.** Experimental flume setup. (a) Photograph. (b) Schematic overview.

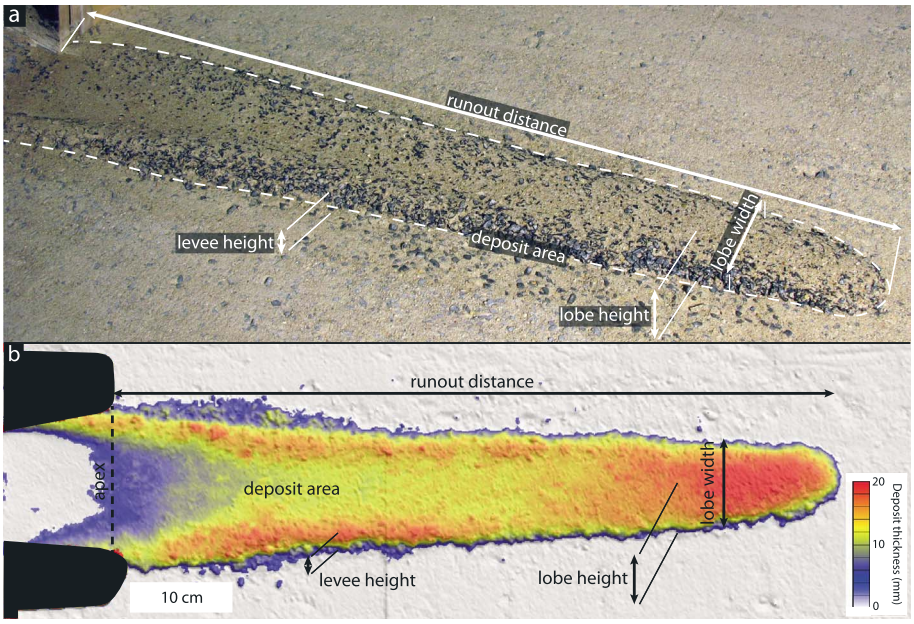


**Figure 2.** Mapped quantities of debris flow deposits; runout distance, deposit area, lobe height, lobe width, and levee height. (a) Picture of debris flow deposit (reference mixture). (b) Hillshade image derived from the DEM of the same deposit.

Multiple cameras were used to photograph debris flow deposits and capture debris flow motion. Debris flow deposits were photographed with a Canon PowerShot A640 camera suspended above the flume. Debris flow velocity was inferred from movies shot with a Canon Powershot A650 IS camera. Flow depth was measured near the channel apex, from a movie shot with a Canon Powershot A650 IS that captured a tape measure (accuracy ~2–3 mm). Flow depth was only measured in the last 58 experiments.

Deposit morphology was measured with a Vialux z-Snapper 3-D scanner that captured a high-accuracy 3-D point cloud from a fringe pattern projector and camera (submillimeter vertical and horizontal accuracy) [*Hoefling*, 2004]. Point clouds from the 3-D scanner were processed with MATLAB (The MathWorks, version 7.13.0.564) using natural neighbor interpolation to a gridded DEM of 1 mm resolution. The DEM was used for visualization and to measure runout distance and area, lobe width, lobe height, and levee height (Figure 2). Runout distance was defined as the distance from the apex to the maximum extent of the debris flow. Deposit area was defined as the total area of the debris flow deposit on the outflow plain. We characterized lobe height as its maximum value and lobe width as the point where its sides became approximately parallel, upstream from its maximum extent. Levee height was measured where levees were well developed, sufficiently downstream of the apex and upstream of the lobe terminus. In cases where levee height varied considerably, we averaged over multiple measurements along the flow deposit.

### 2.3. Debris Flow Composition

The debris flow mixtures were composed of four basic sediments, combined in different ratios. These were clay (kaolinite), well-sorted fine sand, poorly sorted coarse sand, and basaltic gravel (2–5 mm) (Figure 3). The bulk of the mixture generally consisted of sand (Figure 3c). The dark-toned gravel conveniently highlighted textural patterns within the debris flows. The gravel in our experimental debris flows behaved similar to the coarse-grained fraction (typically cobble- to boulder-sized debris) in natural debris flows, in the sense that it formed the coarse-grained flow front and levees. To clarify discussion and comparison between experimental results and nature, we therefore use coarse-grained fraction and gravel fraction as synonyms throughout the text.

The reference sediment mixture consisted of 100 g clay, 1050 g fine sand, 2950 g coarse sand, and 900 g gravel, mixed with 1500 g of water (Figure 3a). We varied the fractions of gravel and clay in the sediment mixture (Figure 3b) but kept the total amount of sediment constant (5000 g). Debris flow volume only varied in the set of experiments where volume was explicitly varied and in one set of experiments wherein the amount of water was varied to evaluate the effect of water to sediment ratio (Table 1).

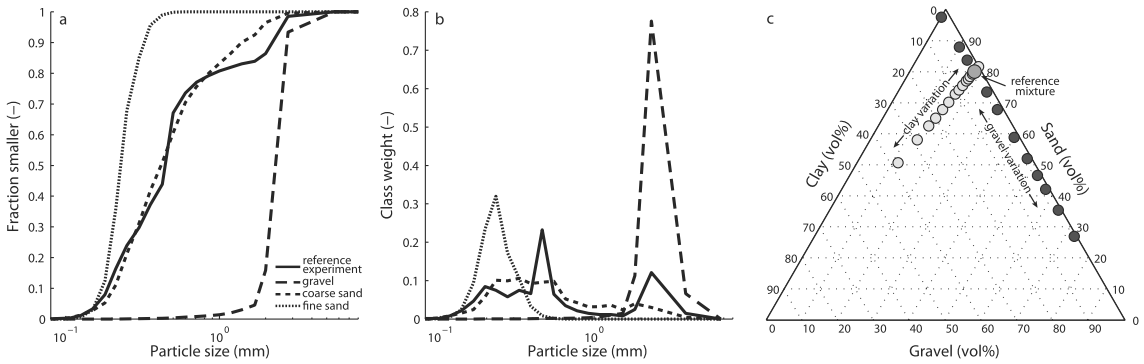


**Figure 3.** Sediment textures. (a) Cumulative particle size distribution of individual sediment components that were combined to form debris flow sediment compositions and the reference mixture. Clay (kaolinite) was the fourth component. (b) Frequency distribution of the sediment components shown in Figure 3a. (c) Ternary diagram indicating the relative volumetric contribution of clay, sand (fine- and coarse-sand components combined), and gravel of the various sediment compositions used in the experiments.

### 2.4. Geotechnical Properties

In independent tests we measured the permeability and diffusivity of the debris flow mixtures. As these measurements were performed in independent tests, they represent the characteristics of the sediment after release from the mixing tank before grain size segregation occurred.

Permeability of the debris flow mixtures was measured with a constant head permeameter [e.g., *Klute and Dirksen*, 2003] (see also the American Society for Testing and Materials D2434 method procedure). A similar amount of sediment and water as used in the experiments was mixed and then poured in a crate, with a permeable mesh at the bottom and sides to stimulate drainage. After 20 min, five samples were obtained from the deposits for analysis in the permeameter.

Diffusivity was measured with the method of *Major* [2000]. We used a smooth-walled, 0.125 m diameter transparent tube in vertical position with an impermeable floor, which we filled to a height of approximately 0.55 m with a well-mixed sediment mixture. Pore fluid pressures were measured at 0.05, 0.15, 0.25, and 0.45 m above the bed. Excess fluid pressure was determined by subtracting hydrostatic fluid pressure from measured total fluid pressure. Hydrostatic fluid pressure $P_h$ (Pa) was calculated as

$$P_h = \rho_f g(h - z) \tag{1}$$

where $z$ is height above the bed (m), $h$ is deposit thickness (m), and $g$ is acceleration due to gravity (9.81 m/s$^2$). The mass density of the interstitial fluid $\rho_f$ is defined as the mass densities of pure water $\rho_w$ (1000 kg/m$^3$) and fines (silt and clay) combined ($\rho_s$, assumed 2650 kg/m$^3$) [cf. *Iverson*, 1997]:

$$\rho_f = \rho_s v_{\text{fines}} + \rho_w(1 - v_{\text{fines}}) \tag{2}$$

where $v_{\text{fines}}$ is the volume fraction of the interstitial fluid occupied by fines. The decrease of excess fluid pressure as fluid moves out of the mixture and sediment settles is described by the following relation [*Major*, 2000]:

$$P_\star = 8P_{\star 0}\sum_{n=0}^{\infty}\frac{1}{(2n+1)^2\pi^2}\cos(\lambda_n z)\mathrm{e}^{-\lambda_n^2 Dt} \tag{3}$$

where $D$ is the diffusion coefficient (m$^2$/s), $P_\star$ is the measured excess fluid pressure (Pa) at $z$, and $t$ is time of measurement relative to start of the experiment (s). The eigenvalues $\lambda_n$ are defined as

$$\lambda_n = \frac{(2n+1)\pi}{2h} \tag{4}$$

$P_{\star 0}$ represents the initial excess pore fluid pressure (Pa) at $z = 0$ in a fully saturated mixture:

$$P_{\star 0} = (\rho_s - \rho_f)(1 - v_f)g(h - z) \tag{5}$$

where $\rho_s$ is the mass density of solid particles (2650 kg/m$^3$). The volumetric interstitial fluid fraction $v_f$ is the combined volumetric fraction of pure water fraction and fines (silt and clay), which equals the porosity in a

saturated mixture [*Iverson*, 1997]. We empirically determined the value of the diffusion coefficient $D$ by iteratively minimizing the difference between measured and predicted excess fluid pressure averaged over all depths [cf. *Major*, 2000].

Geotechnical properties were not measured for every debris flow sediment composition used. For the calculation of dimensionless parameters denoting flow regime and scaling (sections 2.5 and 2.6) we fitted (linearly or exponentially, depending on the data trend) the missing values based on measured values. The same was done for missing values of flow depth.

### 2.5. Dimensionless Characterization of Flow Regime

*Iverson* [1997], *Iverson and Denlinger* [2001], *Iverson et al.* [2010], and *Iverson* [2015] present a set of dimensionless parameters to describe debris flow regime. These allow comparisons between debris flows of different sizes and scales and enable quantitative assessment of the similarity in flow regime of experimental to natural debris flows. Here we summarize these parameters.

There are three forces that resist motion in debris flows: collisional, frictional, and viscous forces [*Iverson*, 1997; *Parsons et al.*, 2001; *Iverson and Denlinger*, 2001]. Three dimensionless parameters describe the relationship between these forces. The Bagnold number defines the ratio of collisional to viscous forces:

$$N_B = \frac{v_s \rho_s \delta^2 \gamma}{(1 - v_s)\mu} \tag{6}$$

wherein $\delta$ is the mean grain size of a debris flow mixture (m) [cf. *Iverson*, 1997], $v_s$ is the volumetric solids fraction and $\gamma$ is the flow shear rate (1/s):

$$\gamma = \frac{u}{H} \tag{7}$$

wherein $u$ is flow velocity (m/s) and $H$ is flow depth (m). We estimate the interstitial fluid viscosity $\mu$ as [*Thomas*, 1965, cf. *Iverson*, 1997]

$$\mu/\mu_w = 1 + 2.5 v_{\text{fines}} + 10.05 v_{\text{fines}}^2 + 0.00273 \exp(16.6 v_{\text{fines}}) \tag{8}$$

where $\mu_w$ is the dynamic viscosity of pure water (0.001002 Pa s).

The ratio of collisional to frictional forces is defined by the Savage number:

$$N_S = \frac{\rho_s \delta^2 \gamma^2}{(\rho_s - \rho_f) g H \tan \phi} \tag{9}$$

wherein $\phi$ is the internal angle of friction (assumed 42°) [cf. *Parsons et al.*, 2001]. The ratio of frictional to viscous forces is defined by the friction number:

$$N_F = \frac{v_s (\rho_s - \rho_f) g H \tan \phi}{(1 - v_s)\gamma \mu} \tag{10}$$

*Iverson* [1997] constrains the magnitudes at which these dimensionless parameters transition from one force being dominant over the other, mostly based on experiments of cohesionless dry flows with unimodal spherical particles [*Bagnold*, 1954; *Savage and Hutter*, 1989]: collisional forces dominate over viscous forces for $N_B > 200$, collisional forces dominate over frictional forces for $N_S > 0.1$, and frictional forces dominate over viscous forces for $N_F > 2000$. In contrast, experimental data of water-saturated small-scale debris flows of *Parsons et al.* [2001] suggest that frictional forces start dominating viscous forces at $N_F > 100$ for the flow body and $N_F > 250$ for the flow front. We test both transitions against our data in section 3.2.

The ratio of solid inertia to fluid inertia is described by the mass number [*Iverson*, 1997]:

$$N_M = \frac{v_s \rho_s}{(1 - v_s)\rho_f} \tag{11}$$

Although no experimental data on the transition values of $N_M$ are available, its qualitative influence is obvious from its definition: grain inertia becomes unimportant as the density or concentration of grains approaches zero. Natural grain density has a relatively narrow range compared to other variables, however. The effect of the proportion of water in the flow will be assessed experimentally.

The Darcy number ($N_D$) describes the tendency for pore fluid pressure to buffer grain interactions:

$$N_D = \frac{\mu}{v_s \rho_s \gamma k} \tag{12}$$

wherein $k$ is permeability (m$^2$). *Iverson and LaHusen* [1989] reported experiments with $1000 < N_D < 6000$, in which large fluid pressure fluctuations evidenced strong solid-fluid interactions. Following *Iverson* [1997], we assume that values of $N_D$ in this range apply to debris flows.

The grain Reynolds number compares the effects of particle collisions and pore fluid viscosity [*Iverson*, 1997]. It defines the ratio between the solid inertial stress and the fluid viscous shearing stress:

$$N_{Rg} = \frac{N_B}{N_M} = \frac{\rho_f \gamma \delta^2}{\mu} \tag{13}$$

Typically, fluid flow with respect to grains begins to show inertial effects and deviates significantly from ideal viscous behavior for $N_{Rg} > 1$ [*Vanoni*, 1975].

### 2.6. Dimensionless Characterization of Scaling

*Iverson and Denlinger* [2001], *Savage and Iverson* [2003], and *Iverson et al.* [2010] show how scale-dependent behavior, which potentially causes scale effects in small experiments, can be assessed by several dimensionless parameters. The parameter $N_R$ provides a measure of the influence of viscous effects relative to flow size:

$$N_R = \frac{\rho H \sqrt{gL}}{\mu} \tag{14}$$

where $\rho$ is the mass density of the debris flow mixture (here about 1920 kg/m$^3$) and $L$ is the maximum length of the flow mass (m), here assumed equal to the channel length. Viscous effects will be less important in large flows (i.e., those with large $H\sqrt{gL}$) than in small flows with the same dynamic viscosity $\mu$ [*Iverson and Denlinger*, 2001].

The parameter $N_P$ expresses the ratio of timescales for debris flow motion and pore pressure diffusion:

$$N_P = \frac{\sqrt{L/g}}{H^2/D} \tag{15}$$

Values of $N_P << 1$ apply in most geophysical flows and indicate that if high pore pressure (i.e., excess pore pressure) develops, it persists much longer than the time needed for downslope grain flow motion. Moreover, because $N_P$ decreases quadratically as the flow thickness $H$ increases, large-scale flows preserve high pore pressures much longer than small-scale flows with the same mixture composition. The difference in pore pressure diffusion between large-scale and small-scale debris flows may therefore affect flow dynamics [*Iverson and Denlinger*, 2001].

## 3. Results

In this section we first describe flow behavior, deposit morphology, and sediment sorting in the experimental debris flows with various compositions. Then flow regimes of the debris flows with various compositions are discussed in terms of dimensionless numbers. Next, we identify effects of debris flow composition and initial conditions of debris flow volume and topography on runout distance and deposit morphology and geometry. We evaluate the effect of flow momentum on runout and deposit geometry. Finally, we assess the effect of outflow plain bed composition.

### 3.1. Flow Behavior, Deposit Morphology, and Sediment Sorting

Multiple flow surges were observed in the debris flows, and coarse particles were observed to concentrate at the flow front in the majority of experimental debris flows (Movies S1–S8 in the supporting information). When entering the outflow plain, the flow front was continuously shouldered aside into lateral levees. The levees then laterally confined the flow to form elongate debris flow deposits. Segregation into more resistive gravelly flow fronts and finer-grained, more dilute, tails was observed in these debris flows. Only in debris flows with a very high clay fraction (>0.22), where viscous forces increasingly dominated over collisional and frictional forces, did coarse particles not accumulate at the flow front. In those flows levees did not form, which caused the debris flows to spread laterally after leaving the channel (Movie S5).

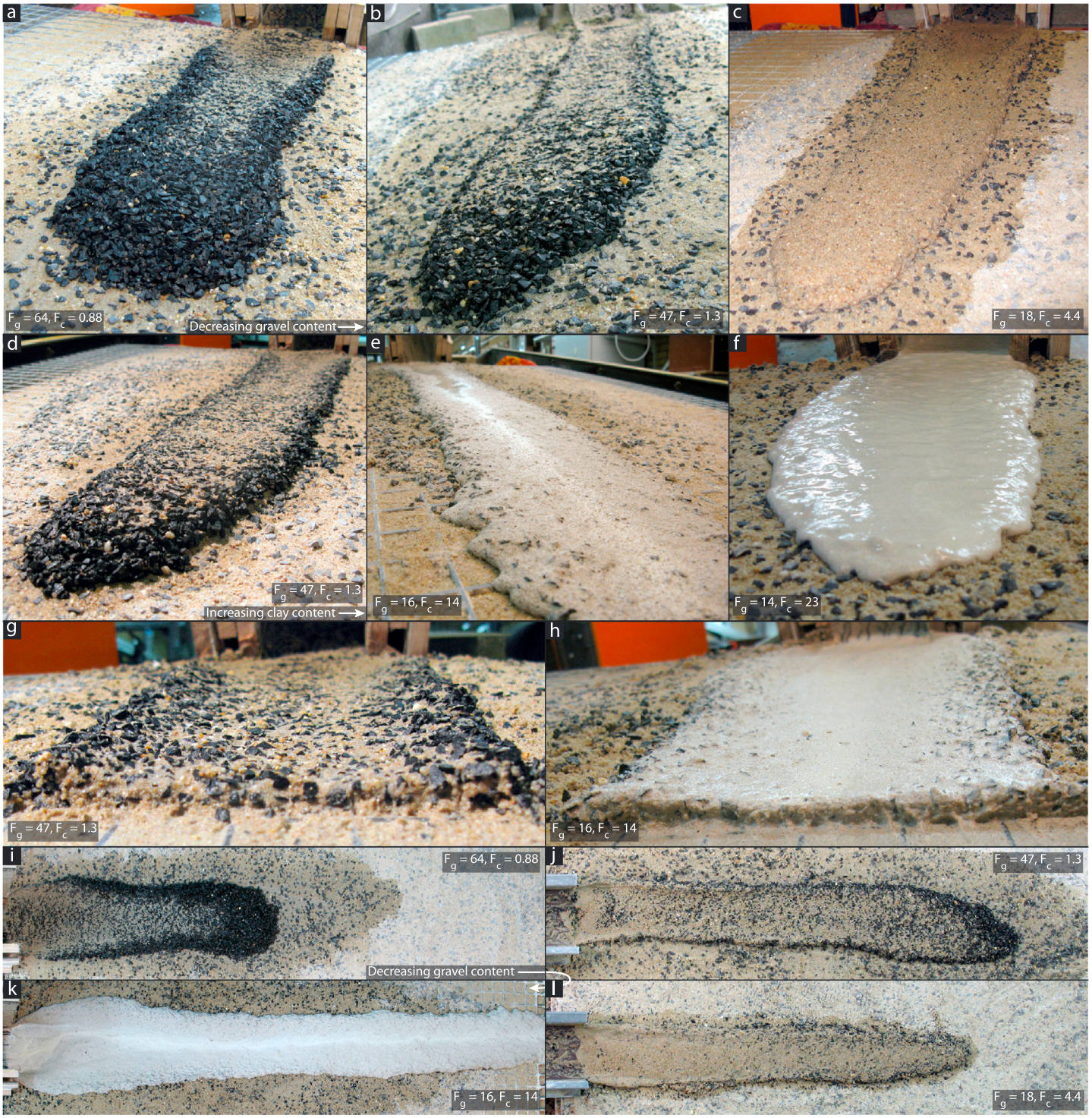


**Figure 4.** Morphology and sediment sorting of selected experimental debris flows. (a–c) Oblique photographs of debris flows with decreasing gravel content. The coarse-grained frontal accumulation decreases with decreasing gravel concentration, and grain size segregation becomes less evident. (d–f) Oblique photographs of debris flows with increasing clay content. Grain size segregation decreases with increasing clay content and eventually is inhibited when flows become viscous (Figure 4f). (g and h) Cross sections highlighting particle size difference between levees and channel. (i–l) Top view photographs highlighting changes in debris flow runout and texture with decreasing gravel content and increasing clay content. $F_g$ refers to vol % of gravel, and $F_c$ refers to vol % of clay. Details on experimental debris flows are in Table S1.

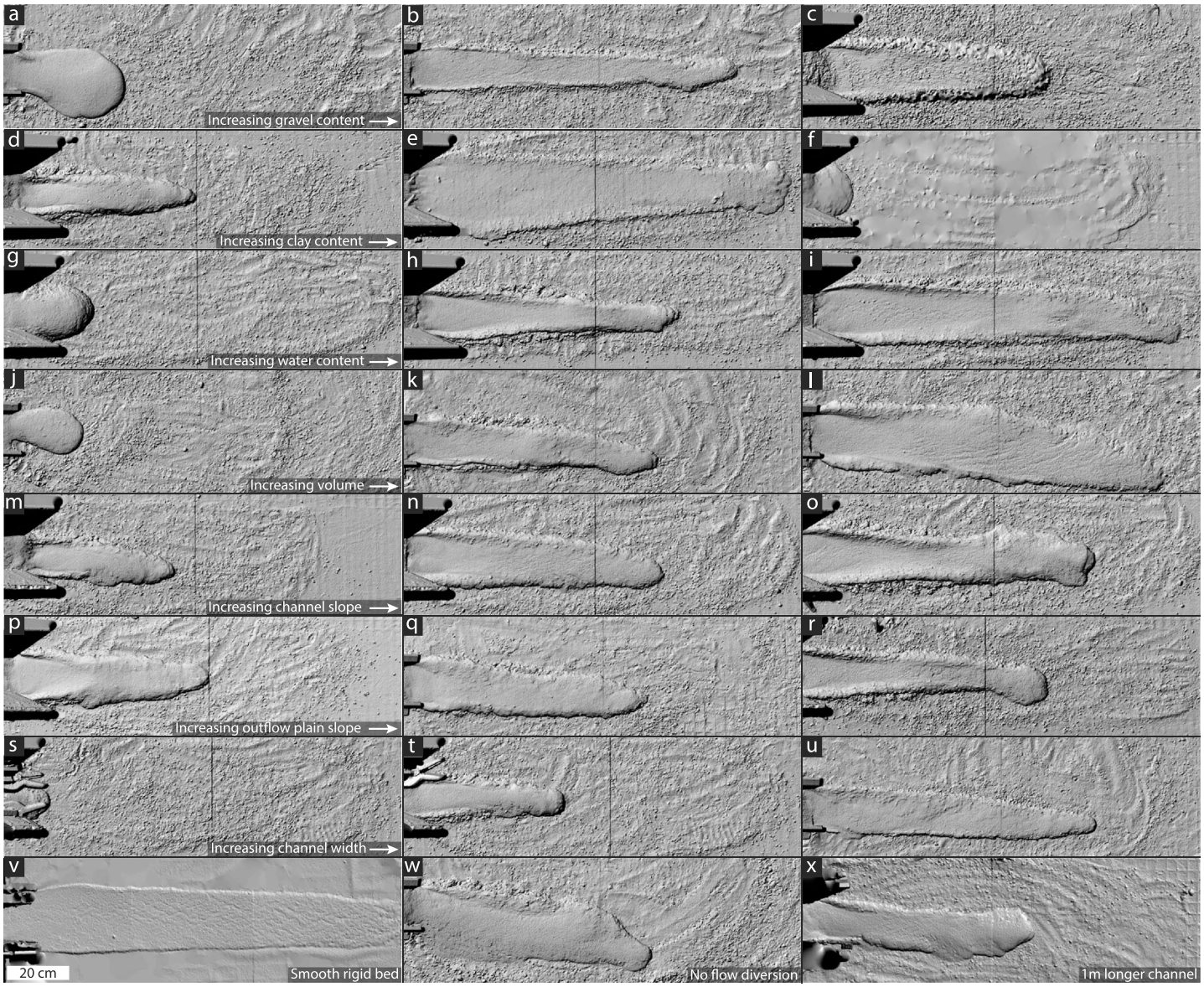


**Figure 5.** Hillshade images of selected debris flows. (a–c) Variable gravel content: 0, 23, and 49 vol % gravel, respectively. An initial increase in gravel content enhances runout, but above an optimum value runout is reduced. (d–f) Variable clay content: 0, 11, and 22 vol % clay, respectively. Adding clay to the debris flows initially enhances runout, but above a threshold of ~22 vol % runout decreases dramatically. (g–i) Variable water content: 41, 44, and 51 vol %, respectively. Increasing water content enhances runout. (j–l) Volume variation: 0.0020, 0.0034, and 0.0051 $m^3$, respectively. Increasing debris flow volume enhances runout. (m–o) Variable channel slope: 24°, 28°, and 34°, respectively. Debris flows run out longer on steeper channel slopes. (p–r) Variable outflow plain slope: 0°, 10°, and 15°, respectively. Debris flow runout is larger on steeper outflow plain slopes. (s–u) Channel width variation: 4.5, 9.5, and 12 cm wide, respectively. An increase in channel width from 4.5 to 12 cm increases debris flow runout. (v) Smooth and rigid outflow plain bed. Long and wide runout, a thin deposit and no levees and grain size segregation. (w) No diversion of debris flow tail results in filling of the leveed channel and in a few cases a little overflow of the channel. (x) Longer channel, 3 m instead of 2 m. A longer channel does not discernably influence runout and deposit morphology. Figures 5v–5x can be compared to reference experiments shown in Figures 5h, 5k, and 5q, which have similar composition.

Under a wide range of conditions debris flows formed deposits that consisted of a channel bordered by self-formed lateral levees. These ended in a well-defined depositional lobe (Figures 4 and 5), with coarse gravel particles concentrated in lateral levees and at lobe margins. Thus, in most deposits there was a marked difference in particle size between the deposit margins and interior. Deposit interiors contained much finer particles, both at the surface (Figures 4a, 4b, 4d, and 4i) and in cross section (Figure 4g). Similar, although less pronounced, sorting patterns were present in debris flows with a relatively high clay fraction (Figures 4e, 4h, and 4k). However, in debris flows for which the clay fraction exceeded 0.22, distinct particle size sorting

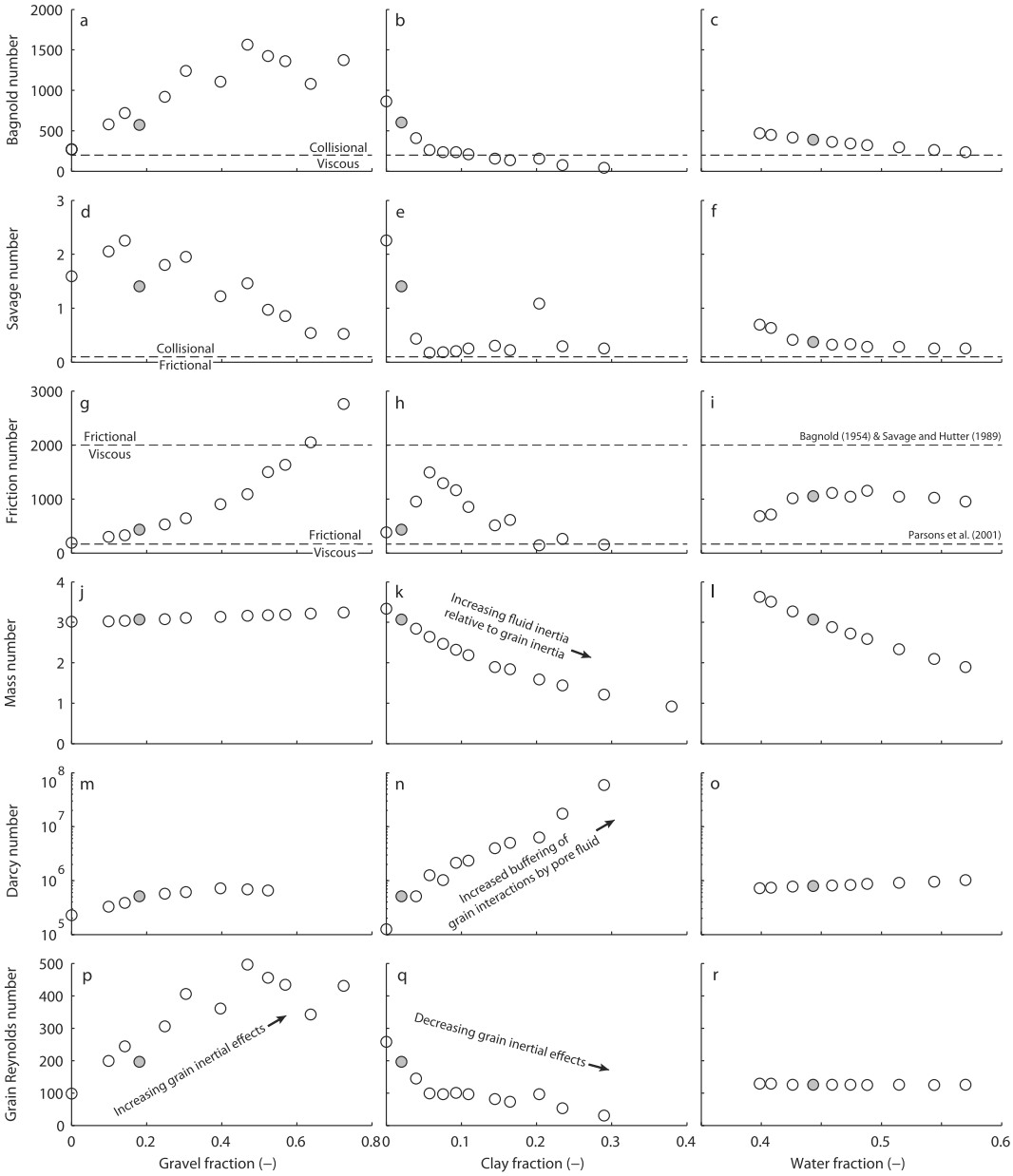


**Figure 6.** Flow regime of experiments with varying gravel, clay, and water fraction. Data points are experimental results averaged per parameter. The majority of the experimental debris flows was observed to have a frictional flow regime given the effective grain size segregation [*Vallance and Savage*, 2000]. Flows with a clay fraction >0.22 had a viscous flow regime. The *Parsons et al.* [2001] boundary in Figures 6g–6i between dominant frictional and viscous forces is thus more accurate for our experimental debris flows than the boundaries proposed by *Bagnold* [1954] and *Savage and Hutter* [1989]. The exceptionally large Savage number for a clay fraction of 0.20 in Figure 6e results from a relatively large shear rate, caused by relatively high flow velocity and low flow depth. Reference experiments are indicated by gray fill.

was absent (Figure 4f). This was probably caused by the high viscosity of these debris flows, wherein grain interactions are effectively buffered by a highly viscous pore fluid (see section 3.2).

### 3.2. Flow Regime

Accumulations of coarse particles in lateral levees and frontal margins were observed in all debris flow deposits, except for those with clay fractions exceeding 0.22. Grain size segregation occurs in frictional flows but is inhibited in collisional or viscous flows [*Vallance and Savage*, 2000]. Frictional grain interactions promote grain size segregation, whereas diffusive mixing hampers segregation in collisional flows and the damped turbulence inhibits percolation and thus segregation in viscous flows [*Vallance and Savage*, 2000]. This implies

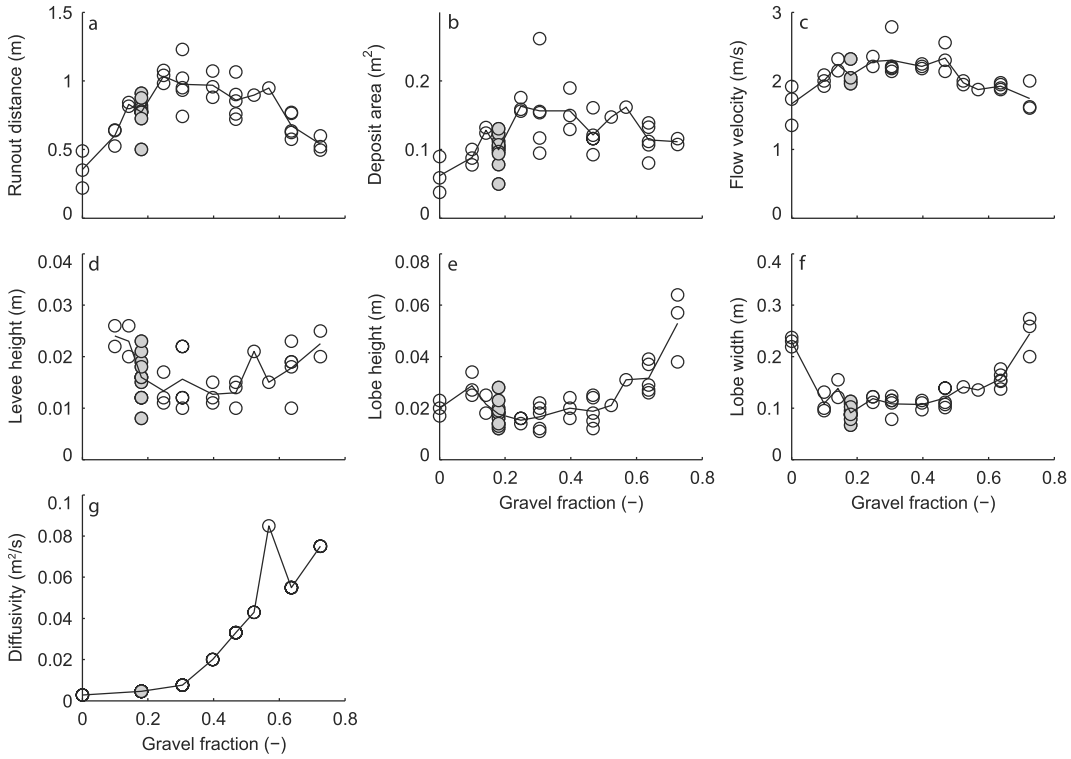


**Figure 7.** Flow, morphological, and geotechnical properties as a function of gravel fraction in otherwise the same conditions. The solid line connects the mean values calculated for each gravel fraction class. Reference experiments are indicated by gray fill.

that the experimental debris flows were frictional flows, except for flows with clay fractions >0.22, which behaved as viscous flows.

Most experiments, except those with the highest clay fractions, plot above the transition from viscous to collisional flow regimes and the transition from frictional to collisional flow regimes proposed by *Bagnold* [1954] and *Savage and Hutter* [1989] (Figures 6a–6f). However, observations from debris flow deposits imply that frictional forces dominated over collisional forces in these experiments. This suggests that the boundaries proposed by *Bagnold* [1954] and *Savage and Hutter* [1989], which are based on dry flow experiments and applied to debris flows by *Iverson* [1997], are not applicable to our experimental debris flows. This is further supported by the boundaries proposed for the transition between viscous and frictional flow regimes (Figures 6g–6i). Here the transition proposed by *Bagnold* [1954] and *Savage and Hutter* [1989] erroneously suggests that the vast majority of the flows had a viscous flow regime. Only the debris flows with clay fractions >0.22 had a viscous flow regime. This transition coincides with the transition proposed by *Parsons et al.* [2001], which is based on debris flow experiments. The boundary proposed by *Parsons et al.* [2001] thus more accurately describes the flow regime of our experimental debris flows. These results suggest that the boundaries between viscous, frictional, and collisional flow regimes vary significantly between dry grain flows and water-saturated debris flows.

In debris flows with high clay fractions the effect of fluid inertia outweighs grain inertia (Figures 6k and 6q) and grain interactions become more effectively buffered by viscous pore fluid (Figure 6n), which causes grain inertial effects to decrease (Figure 6q). This is due to the suspension of clay in the pore water, which enhances pore fluid viscosity. A higher water fraction results in a slight decrease in the effect of collisional forces relative to viscous and frictional forces (Figures 6c and 6f). The effect of frictional forces becomes more important relative to viscous forces with increasing water content (Figure 6i), and fluid inertia becomes more important relative to grain inertia (Figure 6l). The relative influence of grain inertial effects increases with increasing gravel concentration (Figure 6p).

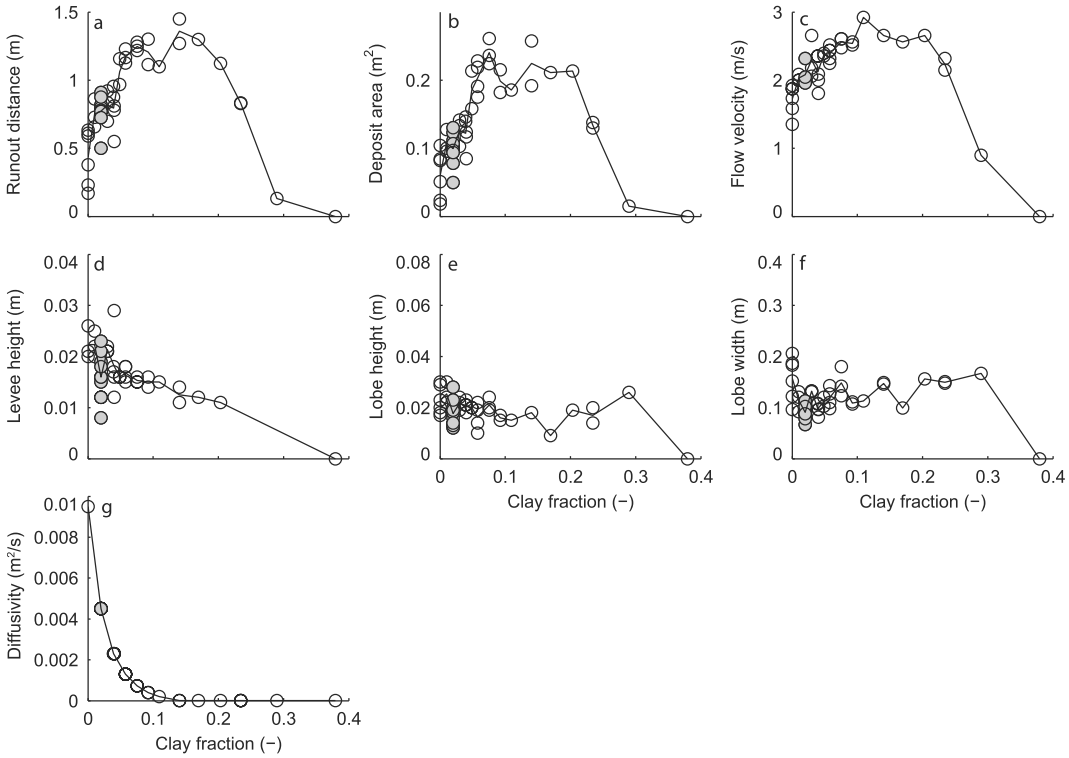


**Figure 8.** Flow, morphological, and geotechnical properties as a function of clay fraction in otherwise the same conditions. See Figure 7 for legend.

### 3.3. Effects of Debris Flow Composition on Runout Distance and Deposit Morphology

#### 3.3.1. Effects of Coarse-Grained Fraction

Runout distance varied between 0.2 and 1.2 m, for gravel fractions in the debris flows ranging from 0 to 0.72 (Figures 7 and 5a–5c and Movies S1–S3). The longest runout distance occurred for intermediate gravel fractions between 0.25 and 0.5 (Figure 7a), whereas both lower and higher gravel fractions led to shorter runout distances. A similar trend was observed for deposit area, which was also largest for intermediate gravel fractions (Figure 7b). We observed that the optimum runout was related to grain size segregation: at low gravel concentrations levees were insignificant, which allowed lateral spreading and reduced longitudinal runout, whereas high gravel concentrations increased gravel accumulation at the flow front, which reduced runout distance, probably due to increased frictional resistance at the flow front (Figures 4a–4d, 4i, 4j, and 4l).

Flow momentum influenced runout distance and area. The highest flow velocities occurred at the optimal gravel fractions but were lower for both lower and higher gravel fractions (Figure 7b). The decrease in velocity for high gravel fractions was likely caused by the high frictional resistance in the coarse-grained flow front and possibly by increased pore fluid loss due to higher diffusivity (Figure 7g). At low gravel fractions driving collisional forces were probably low, leading to a relatively low flow velocity (Figure 6a).

Lobe height and width were also strongly determined by gravel fraction and resultant grain size segregation (Figures 7e and 7f). Larger gravel concentrations led to larger accumulations of gravel at the terminal flow margins and consequently higher lobes. Low gravel concentrations led to wide lobes because levees could not form and confine the flow. The trend for levee height was similar to but less pronounced than the trend for lobe height versus gravel fraction (Figure 7d).

#### 3.3.2. Effects of Clay Fraction

Clay fraction varied from 0 to 0.38 in the experimental debris flows (Figures 8 and 5d–5f and Movies S1, S4, and S5). Maximum runout distance was 1.45 m, and a clear runout optimum occurred for debris flows with a clay fraction between 0.05 and 0.20 (Figures 8a and 8b). The largest runout distances and area coincide with the largest flow velocities (Figure 8c). The increase in runout and flow velocity for an increase in clay fractions from 0 to 0.2 probably results from increasingly well retained excess pore pressures (Figure 8g).

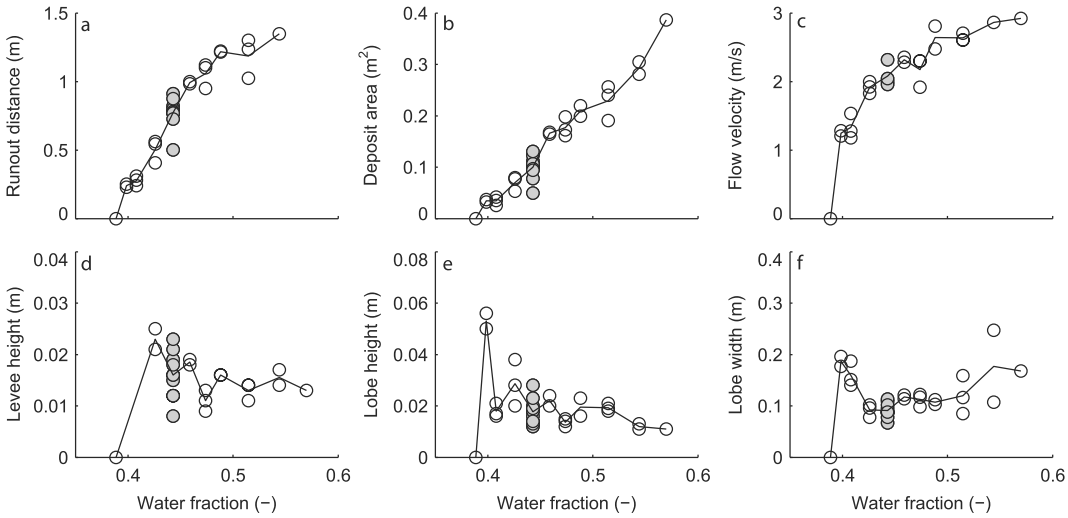


**Figure 9.** Flow and morphological properties as a function of water fraction in otherwise the same conditions. See Figure 7 for legend.

The highly mobile flows with a clay fraction between 0.05 and 0.2 had a relatively dilute appearance (Movie S5); suspending a small fraction of clay in the pore fluid appears to lubricate the flow. Clay fractions $> 0.22$ resulted in viscous flows (Figures 6b, 6e, and 4f), which strongly reduced flow velocity and runout. Moreover, grain size segregation is inhibited in viscous flows, reducing the tendency to form levees that would otherwise increase runout distance. Debris flows with a clay fraction of 0.38 were unable to reach the end of the channel.

Lobe height was inversely proportional to runout (Figure 8e), potentially because longer runout allows less bulking of sediment behind the lobe front as the flows had similar volume. Lobe width, on the other hand, was approximately constant over the entire range of clay fractions (Figure 8f). Levee height strongly decreased for increasing clay fraction (Figure 8d), most likely because levee formation is increasingly inhibited in more viscous flows.

Increasing clay fraction reduced permeability and diffusivity (Figure 8g), preventing pore fluid from escaping the mixture. As a result, we visually observed that debris flow deposits with high clay fractions retained excess pore fluid pressure for long times and needed a long time to consolidate.

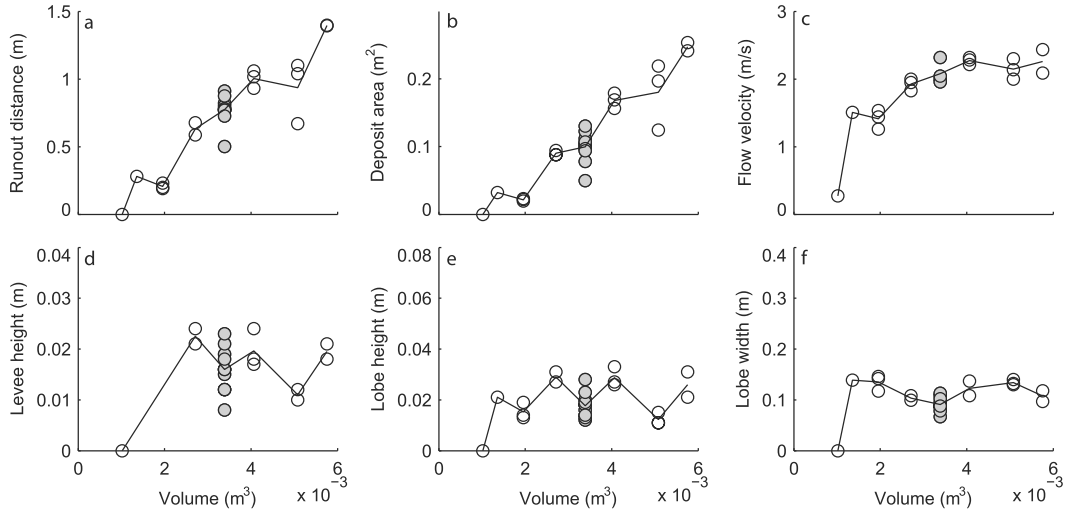


**Figure 10.** Flow and morphological properties as a function of debris flow volume for the reference mixture in otherwise the same conditions. See Figure 7 for legend.

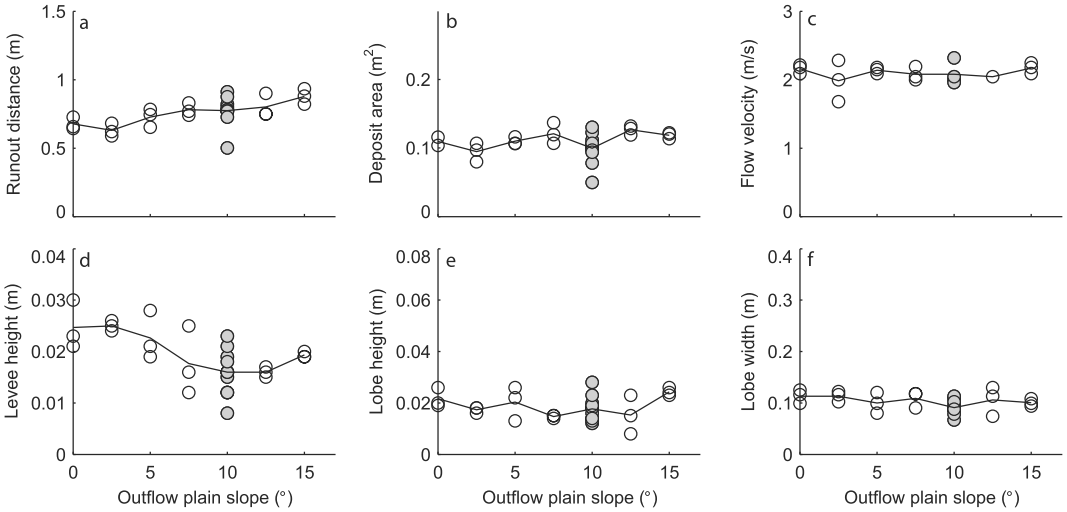


**Figure 11.** Flow and morphological properties as a function of outflow plain slope for the reference mixture in otherwise the same conditions. See Figure 7 for legend.

### 3.3.3. Effects of Water Fraction

Volumetric water fraction in the debris flows varied from 0.39 to 0.57 (Figures 9 and 5g–5i and Movies S1, S6, and S7). Debris flows with a volumetric water fraction of 0.39 or lower were unable to flow to the end of the channel. As pores need to be completely filled with interstitial fluid to cause excess pore fluid pressure, 0.39 possibly approaches the dynamic porosity of the debris flow mixture. A large water fraction led to an increase in runout and flow velocity and thinner deposits. In general, lobe and levee height decreased with increasing water fraction. Lobe width was approximately constant, although width was larger at relatively low and high water fractions (Figures 9f and 5g–5i).

The debris flows were very sensitive to water content: a 10% increase in volumetric water fraction made the difference between no runout on the outflow plain to over 1.2 m runout. The effect of increasing water fraction was slightly enhanced owing to a minor increase in debris flow volume (i.e., water volume was increased and total amount of sediment was kept constant).

### 3.4. Effects of Initial Conditions of Flow Volume and Topography

Debris flow volume varied between 0.0010 and 0.0058 m$^3$ (Figures 10 and 5j–5l). An increase in debris flow volume led to a distinct, nearly linear, increase in runout distance and area. Flow velocity also increased with

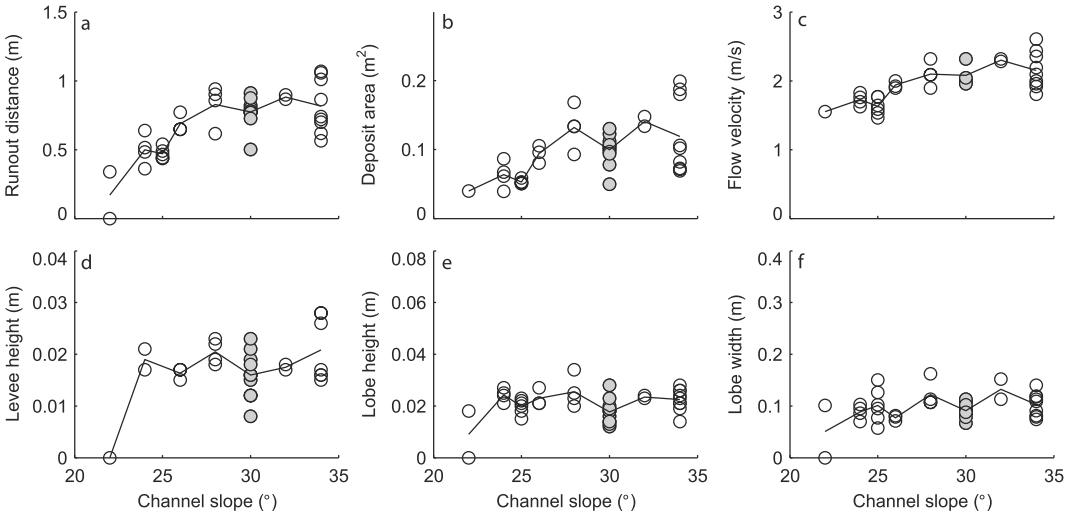


**Figure 12.** Flow and morphological properties as a function of channel slope for the reference mixture in otherwise the same conditions. See Figure 7 for legend.

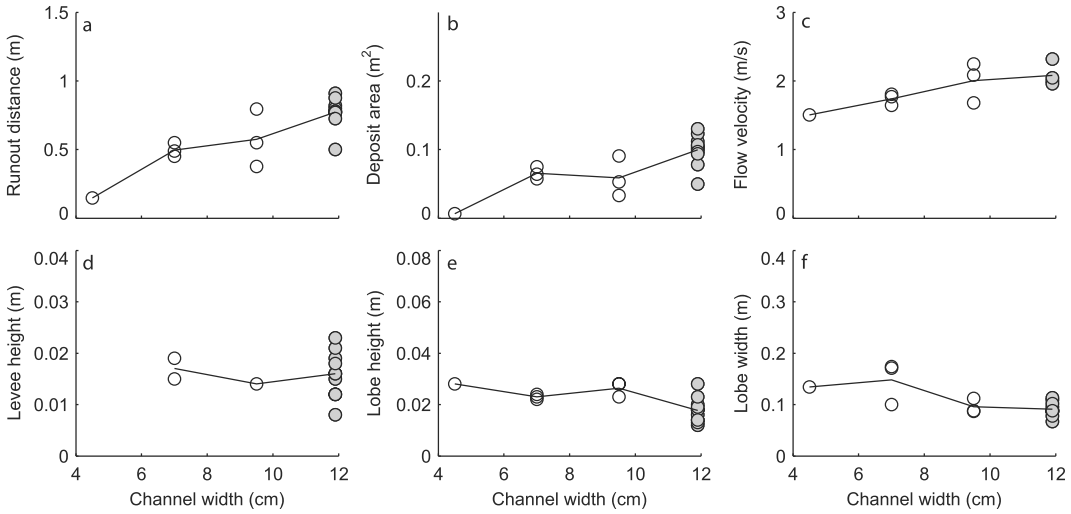


**Figure 13.** Flow and morphological properties as a function of channel width for the reference mixture in otherwise the same conditions. See Figure 7 for legend.

enhanced volume (Figure 10b). The effect of flow volume on levee height, lobe height, and lobe width was negligible (Figures 10c–10e).

Outflow plain slope varied between 0° and 15° (Figures 11c–11e). An increase in outflow plain slope resulted in an increase in runout distance and area, but its effect was relatively small compared to the effects of debris flow composition (i.e., coarse-grained fraction, clay fraction, and water fraction) (Figured 11 and 5p–5r). Deposit morphology was unaffected by the outflow plain slope; levee height, lobe height, and lobe width were similar for various outflow plain slopes.

Channel slope varied between 22° and 34° (Figures 12 and 5m–5o). A steeper channel slope led to larger runout and flow velocities, induced by the increased gravitational potential energy. Levee height, lobe height, and lobe width remained nearly constant (Figures 12c and 12e).

Channel width varied between 4.5 and 12 cm (Figures 13 and 5s–5u). Runout distance and area increased with increasing channel width. A smaller channel width probably led to enhanced wall friction and thereby decreased flow velocity (Figure 13b), reducing runout distances. Levee height, lobe height, and lobe width were largely unaffected by channel width (Figures 13c–13e). Most likely, further increasing channel width will eventually result in a decrease in runout distance because of flow thinning.

Increasing the channel length from 2 m to 3 m, while keeping channel slope constant at 28°, had no discernable effect on debris flow velocity and deposits (Figures 14 and 5x). Flow velocity and runout distance, which are linearly related to each other (Figure 14c), were similar for both channel lengths.

### 3.5. Effects of Flow Momentum on Runout and Deposit Morphology

There is a strong relation between flow momentum, defined as the product of flow velocity and mass, and runout distance and area, regardless of debris flow composition, volume, or terrain geometry

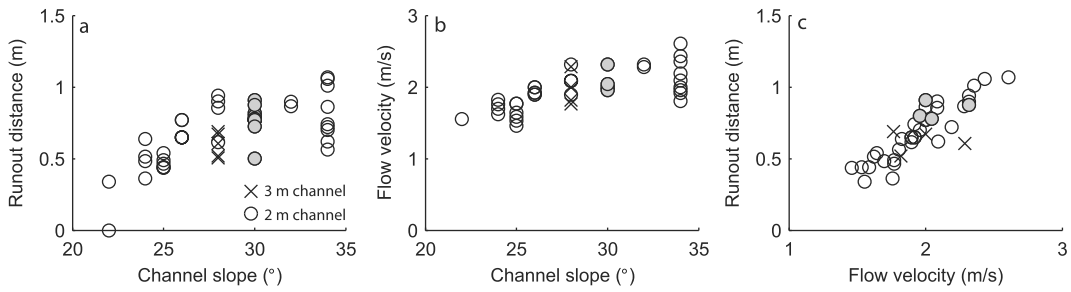


**Figure 14.** Flow and morphological properties as a function of outflow channel length for the reference mixture in otherwise the same conditions. Reference experiments are indicated by gray fill.

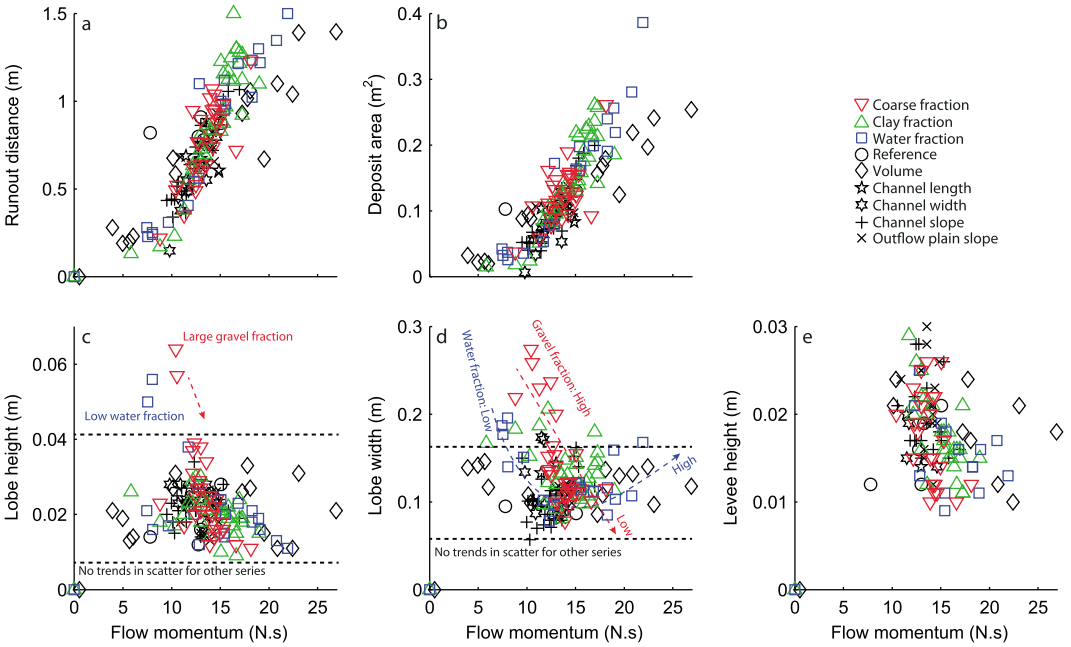


**Figure 15.** Relation between flow momentum and runout distance, deposit area, and deposit morphology. (a) Runout distance versus flow momentum. (b) Deposit area versus flow momentum. (c) Lobe height versus flow momentum. (d) Lobe width versus flow momentum. (e) Levee height versus flow momentum. The different symbols correspond to the different series of varied variables shown in Figures 7–14.

(Figures 15a and 15b). Lobe height and width were largely unaffected by flow momentum (Figures 15c and 15d). However, debris flows of low water fraction and debris flows with a large gravel fraction had a relatively low flow momentum and thick lobe. For both the gravel and water fraction series lobe height decreased and flow momentum increased with increasing water fraction or decreasing gravel fraction, respectively (except for very low gravel fractions). For gravel concentration, this trend probably results from the high frontal friction in debris flows with a high coarse-material fraction. Lobe width was large for low-momentum debris flows with low water fraction. When water fraction increased, flow momentum increased and lobe width decreased because of levee formation. In contrast, when water fraction increased further, lobe width increased again despite a further increase in flow momentum. This was caused by a lack of lateral levee formation,

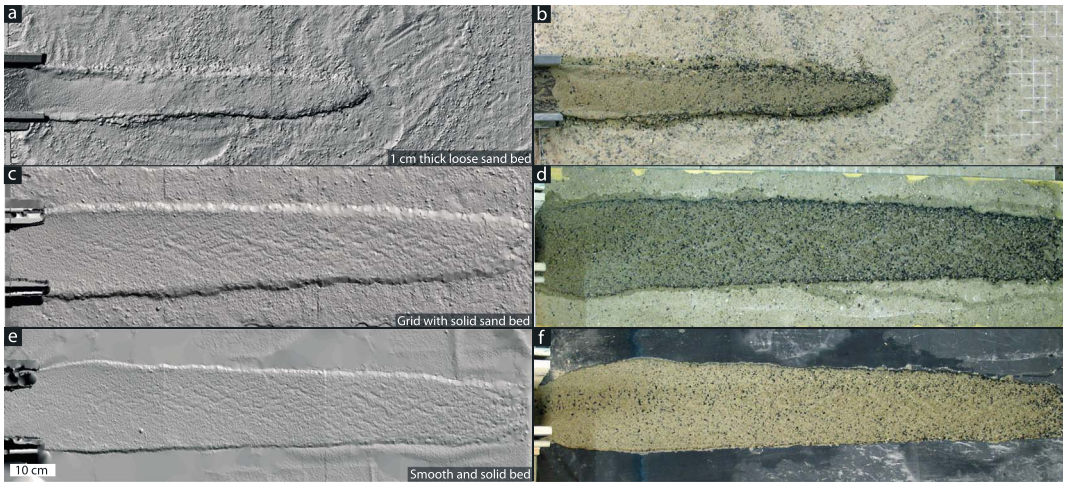


**Figure 16.** Effects of outflow plain bed. (a, b) Initial loose sand bed of ~1 cm thick: deposit with a thick terminal lobe and well-defined coarse-grained lateral levees and frontal lobe margins. (c, d) Fixed sand bed: large runout, lateral spreading, restricted grain size segregation, and small levees. (e, f) Smooth plastic bed: large runout, lateral spreading, no observable grain size segregation, and no discernable levees.

causing lateral spreading of the debris flow and a wide lobe. Levee height decreased with increasing flow momentum for all series (Figure 15e), because runout distance increased and the same amount of sediment was spread over a longer distance.

### 3.6. Effects of Outflow Plain Bed Composition

The presence of a loose, erodible, and porous outflow plain bed resulted in the formation of debris flows with well-developed grain size segregation, levees, and a marked depositional lobe as shown in the previous sections. Figure 16 shows three debris flows for which only the outflow plain surface properties varied. In the presence of a loose initial bed of ~1 cm thickness, the debris flow formed an elongated deposit, with a relatively narrow channel bordered by well-developed levees and a relatively thick depositional lobe. Coarse particles were accumulated in the levees and the lobe margins, and there was a clear particle size difference between the deposit margins and interior (Figures 16a and 16b). Debris flows that flowed over a fixed bed of similar composition, which had comparable roughness but whereon erosion and infiltration were impossible, were more mobile than the debris flows on a loose sand bed. Flow spread laterally and only small levees were formed. Grain size segregation was limited, and only a small fraction of coarse particles concentrated in the levees and at the flow front. A weakly developed thin lobe was formed (Figures 16c and 16d). In the presence of a smooth bed that prevented both erosion and infiltration, lateral spreading of the debris flows was even more dramatic, no grain size segregation occurred, and there was no distinction between channel and lobe (Figures 16e and 16f). Mobility of these flows was similar to the mobility on the fixed sand bed, although slightly more mobile on average.

## 4. Discussion

In this section we discuss effects of debris flow composition on (1) depositional mechanisms, (2) runout, and (3) deposit geometry. We end the discussion with an analysis on the scaling of debris flows in small-scale laboratory flumes.

### 4.1. Debris Flow Deposition

Debris flow deposition can result from numerous processes: (1) decay of excess pore fluid pressure [e.g., *Terzaghi*, 1956; *Hutchinson*, 1986], (2) viscoplastic yield strength [*Johnson*, 1970; *Johnson and Rodine*, 1984; *Coussot and Proust*, 1996], (3) decay of grain collision stresses [e.g., *Lowe*, 1976; *Takahashi*, 1978, 1991], and (4) increasing grain contact friction and friction concentrated at flow margins [*Major*, 1997, 2000; *Major and Iverson*, 1999]. Support for the various hypotheses has been largely anecdotal, however; only the latter hypothesis is based on in situ measurements from replicable, large-scale flume experiments [*Major and Iverson*, 1999].

We did not measure load and pore fluid pressure in the runout zone, and therefore, we can only speculate about the processes that caused deposition in our experiments. However, observations of the size of the coarse-grained accumulation at the flow front, along with diffusivity measurements in static mixtures of the investigated flows, suggest that deposition in most of our experimental debris flows is mainly influenced by friction at the frontal flow margins imposed by the accumulation of coarse particles and decay of pore fluid pressure. Escape rates of pore fluid increased with decreasing clay fraction and increasing gravel fraction, as can be visually observed in the supporting information Movies S1–S8. The importance of frontal friction and decay of pore fluid pressure is best illustrated by the relation between gravel fraction and runout (Figures 7a and 7b); a large gravel concentration leads to a large accumulation of coarse particles at the flow front and higher diffusivity (Figure 7g), resulting in early deposition and reduced runout. We hypothesize that frontal friction was most important in the majority of the experimental debris flows (except for those with very high gravel and very low clay concentrations), as we observed retained high pore pressure in most of the deposits' flow bodies after deposition (water rapidly escaped the deposits upon a slight increase of loading by gently touching the deposit).

In contrast, in the viscous clay-rich experimental debris flows (clay fraction >0.22) the accumulation of coarse sediments at the flow front is marginal to absent and diffusivity of the static mixtures is very low. Yet runout is greatly reduced in these flows (Figures 8a and 8b). We observed no wetting of bed material adjacent to the debris flow after deposition (Movie S5), suggesting retained pore fluid pressures after deposition. These observations suggest that both friction at the flow front and decay of pore fluid pressure did not significantly contribute to deposition in these debris flows. Rather, deposition was probably determined by high effective viscosity and yield strength in these viscous clay-rich debris flows.

### 4.2. Runout Distance

Trends in debris flow runout were in good agreement with the results obtained in natural flows and other experiments as follows. Similar to empirical relations for natural debris flows [*Rickenmann*, 1999], our experimental results show that runout strongly depends on flow momentum. Observations of natural debris flows show long runout distances especially when effective lateral levees were formed [e.g., *Iverson*, 2003; *Zanuttigh and Lamberti*, 2007], which we also observed in the experiments. However, large accumulations of coarse particles at the frontal flow margins decrease runout distance and area as also found in large experimental debris flows at the USGS flume [e.g., *Major and Iverson*, 1999]. High clay fractions reduce flow velocity and runout above an optimum value in the experiments. Runout distances and areas become larger for increasing water fractions, as also observed in experimental debris flows of *D'Agostino et al.* [2010] and *Hürlimann et al.* [2015]. Additionally, an increase in debris flow volume enhances runout, as often observed for natural debris flows [e.g., *Iverson et al.*, 1998; *Zanuttigh and Lamberti*, 2007; *Griswold and Iverson*, 2008]. Larger channel and outflow plain slopes result in larger runout distances and areas, because of the larger gravitational potential energy, in accordance with observations of natural debris flows [e.g., *Prochaska et al.*, 2008]. However, the increase in runout for a similar increase in slope is much larger for the channel slope than for the outflow plain slope. These results show that the response to both compositional and topographic forcings is similar in our small-scale experimental and large-scale natural debris flows.

Our experiments imply that debris flow runout greatly depends on composition. Water content strongly influences runout, and additionally, the amount of clay and relatively large debris (i.e., the particles that accumulate at the frontal flow margins and form levees) strongly influence runout through debris flow composition. The effects of debris flow grain size distribution are barely directly incorporated in current runout distance prediction methods [e.g., *Hungr*, 1995; *Bathurst et al.*, 1997; *Iverson et al.*, 1998; *Rickenmann*, 1999; *Iverson and Denlinger*, 2001; *Crosta et al.*, 2003; *Berti and Simoni*, 2007; *Tang et al.*, 2012]. In some of the most sophisticated models effects of grain size distribution are incorporated through diffusivity, solid volume fraction, compressibility, and redistribution of pore fluid pressure [*Iverson and George*, 2014; *George and Iverson*, 2014], but the effects of grain size segregation and the development of frictional frontal flow margins are not explicitly incorporated in these models. Debris flow composition differs greatly among sites because of different source material and hydrological conditions. As a result, the various approaches to estimate debris flow runout are often site specific [e.g., *Fannin and Wise*, 2001; *Rickenmann*, 2005]. Therefore, runout prediction methods, especially empirical-statistical methods, should only be applied to sites with similar conditions to those on which their development is based [e.g., *Rickenmann*, 2005; *Hürlimann et al.*, 2008]. Nevertheless, also within the same site or fan, where catchment lithology and hydrological conditions are similar, variations in debris flow composition lead to large variability in runout distances [*Whipple and Dunne*, 1992].

In short, there is no simple and universal runout prediction method, and therefore, there is a need to better understand and describe the depositional characteristics and runout behavior of debris flows [*Scheidl and Rickenmann*, 2010]. Our results show that significant improvements may be made by incorporating the effects of debris flow grain size distribution, but this requires more observations on experimental and natural debris flows.

### 4.3. Deposit Morphology

Debris flows occur in many different environments on Earth. They are generated and deposited on hillslopes, catchments, alluvial fans, and channels that can vary greatly in many characteristics, including morphometry and lithology. Additionally, their frequency, initiation mechanism, volume, and composition can greatly vary between sites [e.g., *Caine*, 1980; *Johnson and Sitar*, 1990]. Most of these debris flows have similar morphology; they often have a channel bordered by lateral levees and ending in depositional lobes. However, it remains poorly understood what determines the geometry of debris flow deposits.

Debris flow deposit geometry is largely controlled by debris flow composition in our experiments: the coarse-grained, clay, and water fractions all have a profound effect on lobe height, lobe width, and levee height, while the effects of topography and volume are negligible (Figures 7–15). Additionally, outflow bed characteristics influenced deposit geometry (Figure 16). Depositional lobe thickness was mainly determined by the height of the frontal accumulation of coarse particles in our experiments, behind which the more fluidal debris flow body incrementally accreted up to the height of the frontal coarse-particle accumulation. Similar dependence between lobe height and frontal coarse-particle accumulation has been observed in natural debris flows [e.g., *Pierson*, 1984]. As an exception, in the experimental debris flows wherein clay


**Figure 17.** Comparison between sediment sorting of experimental and natural debris flows. (a) Coarse-grained levees in an experimental debris flow (experiment 64). (b) Coarse-grained levees in natural debris flows on Svalbard (photograph by E. Hauber). (c) Accumulation of coarse debris at the frontal lobe margins in an experimental debris flow (experiment 64). (d) Accumulation of coarse debris at the frontal lobe margins in a natural debris flow in the Atacama Desert (Chile) (photograph by D. Ventra). Experimental debris flow width = ~12 cm. People for scale on natural debris flows.

fractions exceeded 0.22, high viscosity inhibited grain size segregation and consequently the formation of a coarse frontal accumulation. Yet lobe height slightly increased for higher clay fractions from 0.22 to ~0.3 (Figure 8). We hypothesize that these clay-rich debris flows behaved as Bingham viscoplastic flows [*Johnson*, 1970; *Coussot et al.*, 1998], wherein lobe height was mainly determined by an increasing yield strength for higher clay fractions.

### 4.4. Scaling

Flow behavior, deposit morphology, and particle sorting of our small-scale experimental debris flows were similar to those of natural debris flows, as discussed below. A coarse-grained flow front, followed by more dilute material and formation of lateral levees, observed in our experimental debris flows (Movies S1–S8) is a typical feature of natural debris flows [e.g., *Pierson*, 1986; *Iverson*, 1997; *Zanuttigh and Lamberti*, 2007; *Johnson et al.*, 2012]. The coarse-grained levees and lobe margins found in many of the experimental debris flow deposits are also common in natural debris flow deposits [e.g., *Blair and McPherson*, 1998; *Blair*, 1999] (Figure 17). Furthermore, the well-developed grain size sorting implies that the processes that govern the flow behavior of natural debris flows, such as kinematic sorting, squeeze expulsion, and preferential transport of coarse particles to the flow front [*Vallance and Savage*, 2000; *Gray and Kokelaar*, 2010; *Johnson et al.*, 2012], were also present in our experimental debris flows. This also implies that frictional forces dominated the flow in the majority of our experimental debris flows [*Vallance and Savage*, 2000], as they generally also do in natural debris flows [e.g., *Zhou and Ng*, 2010]. The response of deposit morphology, runout distance, and depositional mechanisms to topographic forcings (i.e., channel slope and outflow plain slope) and internal characteristics (i.e., composition) in our experiments was similar to the response of natural debris flows to these forcings [e.g., *Major and Iverson*, 1999; *Rickenmann*, 2005; *Zanuttigh and Lamberti*, 2007]. These observed similarities between small-scale experimental debris flows and natural debris flows suggest that our small-scale debris flow experiments may efficiently complement field observations to identify many of the controls on natural debris flow behavior and deposits.

Compared to natural debris flows, small-scale experimental debris flows exhibit disproportionately large effects of fluid yield strength, viscous flow resistance, and grain inertia while exhibiting disproportionately

**Table 2.** Physical and Dimensionless Parameters of Small-Scale, Experimental Debris Flows and Large-Scale, Natural Debris Flows[a]

| Parameter | Symbol (Unit) | Small-Scale (This Study) Debris Flows | USGS Flume Debris Flows[b] | Typical Range Natural Debris Flows[b] |
|---|---|---|---|---|
| | | *Physical Parameters* | | |
| Typical grain diameter | $\delta$ (m) | 0.0005–0.002 | 0.001 | $10^{-5}$–10 |
| Flow depth | $H$ (m) | 0.005–0.018 | 0.1 | 0.1–10 |
| Flow velocity | $u$ (m/s) | 0.9–2.9 | 10 | 0.1–20 |
| Flow shear rate | $\gamma$ (1/s) | 105–371 | 100 | 1–100 |
| Solid density | $\rho_s$ (kg/m$^3$) | 2650[h] | 2700 | 2500–3000 |
| Fluid density | $\rho_f$ (kg/m$^3$) | 1000–1533 | 1100 | 1000–1200 |
| Solid volume fraction | $v_s$ (–) | 0.35–0.59 | 0.6 | 0.4–0.8 |
| Fluid volume fraction | $v_f$ (–) | 0.65–0.41 | 0.4 | 0.2–0.6 |
| Fluid viscosity | $\mu$ (Pa s) | 0.001–0.0035 | 0.001 | 0.001–0.1 |
| Friction angle | $\phi$ (deg) | 42[h] | 40 | 25–45 |
| Hydraulic permeability | $k$ (m2) | $1.1\times10^{-16}$–$2.1\times10^{-13}$ | $10^{-11}$ | $10^{-13}$–$10^{-9}$ |
| Hydraulic diffusivity | $D$ (m$^2$/s) | $5.8\times10^{-9}$–$1.2\times10^{-1}$ | $10^{-4}$ [e] | $10^{-8}$–$10^{-2}$ [e] |
| | | *Dimensionless Parameters* | | |
| Savage number | $N_S$ | 0.17–2.25 | 0.2 | 10–7–$10^{0}$ [b,c,f] |
| Bagnold number | $N_B$ | 37–1589 | 400 | $10^{0}$–$10^{8}$ [b,c] |
| Friction number | $N_F$ | 141–2760 | $2\times10^{3}$ | $10^{0}$–$10^{5}$ [b,f] |
| Mass number | $N_M$ | 1.2–3.63 | 4 | 1–10[g] |
| Darcy number | $N_D$ | $3.2\times10^{4}$–$5.9\times10^{7}$ | 600 | $10^{4}$–$10^{8}$ |
| Grain Reynolds number | $N_{Rg}$ | 31–504 | 100 | 0.01–2[b,f] |
| Reynolds number | $N_R$ | $2.3\times10^{4}$–$1.4\times10^{5}$ | $3\times10^{3}$ [d] | $10^{5}$–$10^{7}$ [c,d] |
| Pore pressure number | $N_P$ | 0.003–200 | 0.008[c], $6\times10^{-3}$ [d] | $10^{-6}$–$10^{-1}$ [c,d,f] |

[a]Values were taken or calculated from the source specified in the header unless specified otherwise in the footnotes.
[b]*Iverson* [1997].
[c]*Iverson and Denlinger* [2001].
[d]*Iverson et al.* [2010].
[e]*Major* [2000].
[f]*Zhou and Ng* [2010].
[g]Based on debris flows ranging from 20% to 70% of water by volume.
[h]Estimated values.

little effect of pore fluid pressure (Table 2) [*Iverson*, 1997; *Iverson and Denlinger*, 2001; *Iverson et al.*, 2010]. The dimensionless numbers denoting flow dynamics of our experimental debris flows are generally in the range of values that formed in the large-scale USGS flume and of natural debris flows (Table 2) [*Iverson*, 1997; *Iverson and Denlinger*, 2001; *Zhou and Ng*, 2010]. Yet in our experiments the Bagnold, Savage, and grain Reynolds numbers are relatively large, because of shallow flow and high flow velocity, resulting in a high shear rate, and the relatively large characteristic grain size compared to flow depth.

Geometrically, the experimental debris flows are within the range of natural debris flows (Figure 18). We compare debris flow mobility of our experimental debris flows to natural debris flows by comparing total travel distance $L$ with total elevation difference $E$ (mobility ratio) and by comparing inundated area with volume. Note that inundated area in Figure 18a incorporates both the planimetric channel area and the planimetric deposit area (in contrast, Figures 7–13 show only deposit area). Similarly, the mobility ratio of the experiments is defined as the total travel distance $L$ of a debris flow from initiation point (the mixing tank gate) to its farthest point of deposition (lobe terminus) divided by the associated elevation difference $E$ (rather than the runout distance on the outflow plain as shown in Figures 7–13). The ratio between inundated area and volume of the experimental debris flows is similar to the ratio of natural debris flows (Figure 18a). The best fit regression line for natural debris flows found by *Griswold and Iverson* [2008] connects the experimental and the natural debris flows, and all experimental debris flows fall within the 99% confidence intervals for prediction.

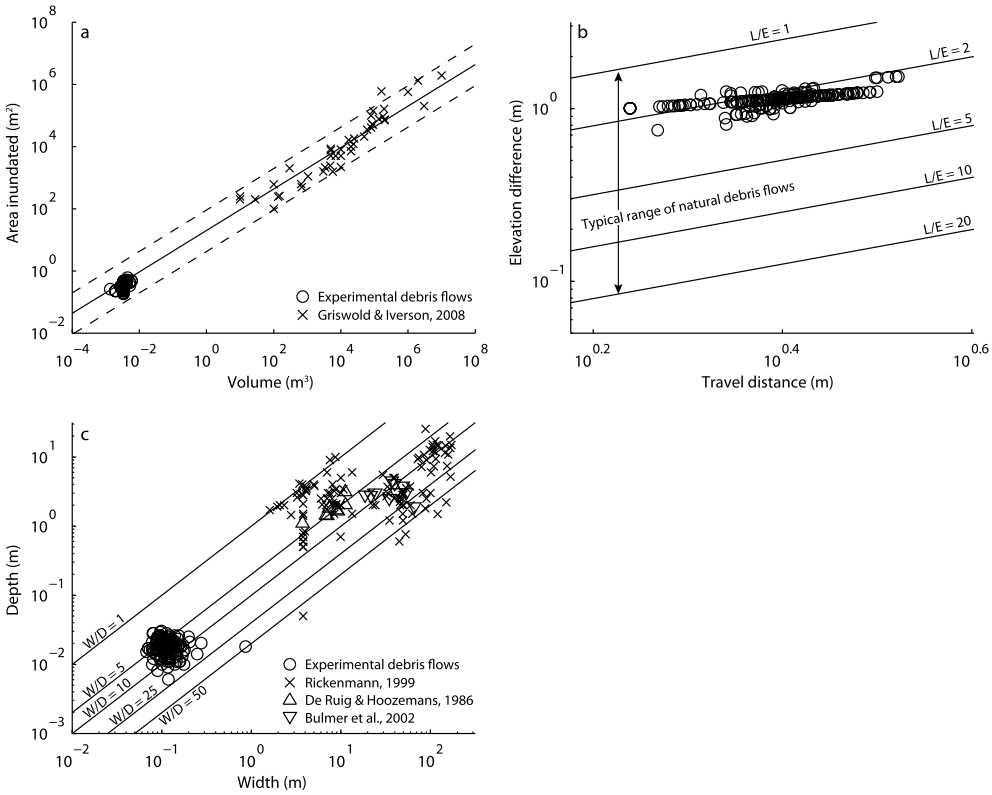


**Figure 18.** Comparison between experimental and unconfined and confined natural debris flow dimensions. (a) Area inundated as a function of debris flow volume for the experimental debris flows and natural debris flows (including the USGS flume data) [*Griswold and Iverson*, 2008]. The solid line is the best fit regression line as reported by *Griswold and Iverson* [2008] ($A = 20V^{2/3}$), and the dashed lines are the 99% confidence intervals for prediction as given by *Griswold and Iverson* [2008]. (b) Mobility ratio ($L/E$), wherein $L$ is the total travel distance of a debris flow from its initiation point to the farthest point of deposition and $E$ is the associated elevation difference. Lines denoting the range of natural debris flow mobility ratio based on values reported in *Corominas* [1996], *Iverson* [1997], *Bathurst et al.* [1997], *Toyos et al.* [2007], and *D'Agostino et al.* [2010]. (c) Debris flow width to depth ratio ($W/D$) (width defined as distance between levees and depth as levee height (Figure 2). Data from natural debris flows from *Rickenmann* [1999], *Bulmer et al.* [2002], and *De Ruig and Hoozemans* [1986].

However, most experimental debris flows fall in the lower end of the spectrum, implying that they are relatively short. Similarly, the mobility ratio of the experimental debris flows is at the lower end of the mobility spectrum observed for natural debris flows. For natural debris flows the mobility ratio typically ranges between 1 and 20 [e.g., *Corominas*, 1996; *Iverson*, 1997; *Bathurst et al.*, 1997; *Toyos et al.*, 2007; *D'Agostino et al.*, 2010], and *Iverson* [1997] suggests that $L/E$ increases logarithmically with increasing volume. The mobility ratio of our experiments ranges from 1.7 to 2.7 (mean = 2.2) (Figure 18b). This suggests that $L/E$ is particularly small for debris flows of small volume [*Iverson*, 1997]. The comparison between the mobility of small-scale experimental and natural debris flows is probably unaffected by the dam break initiation of the experimental debris flows, as runout and flow velocity were similar for a 2 and 3 m channel with a 28° slope (Figure 14). As the runout of a debris flow is a function of travel efficiency and expresses energy dissipation both inside and outside the flow [e.g., *D'Agostino et al.*, 2010], we attribute the relatively short runout distance to the disproportional large effects of fluid yield strength and viscous flow resistance, rapid dissipation of pore pressure [*Iverson and Denlinger*, 2001; *Iverson et al.*, 2010] (Table 2), and the relatively large characteristic grain size compared to flow depth, which together increase the resistance to motion in small-scale debris flows. The width-to-depth ratio of our experimental debris flows fits the range observed in numerous confined and unconfined natural debris flows (Figure 18c).

Many small-scale debris flow experiments have been performed over the past several years, most of which focused on rheology, flow behavior, and the formation of frontal accumulations of coarse debris. Experiments were performed in rotating flumes [*Kaitna et al.*, 2007; *Kaitna and Rickenmann*, 2007], conveyor belt flumes

[*Hirano and Iwamoto*, 1981; *Davies*, 1990; *Hübl and Steinwendtner*, 2000], recirculating flumes [*Armanini et al.*, 2005; *Larcher et al.*, 2007], or open flumes [e.g., *Van Steijn and Coutard*, 1989; *Liu*, 1996; *Parsons et al.*, 2001; *D'Agostino et al.*, 2010, 2013; *Bettella et al.*, 2012; *Hürlimann et al.*, 2015]. In most open flume experiments, debris flows were able to flow out over an unconfined plain; however, no elongate deposits with well-developed self-formed levees and depositional lobes were formed. Rather, large and wide unconfined depositional lobes that spread both in longitudinal and lateral directions were formed [*Van Steijn and Coutard*, 1989; *Liu*, 1996; *D'Agostino et al.*, 2010, 2013; *Bettella et al.*, 2012], similar in morphology and particle sorting to the flows we produced in the absence of a loose erodible bed (Figures 16c–16f). This can probably be attributed to the rigid and often smooth bed of the outflow plains used in these experiments. The necessity of a loose initial bed for the formation of well-developed self-formed levees and grain size segregation probably is a scale effect, as well-developed self-formed levees and grain size segregation occurred in debris flows running over the smooth bed of the large-scale USGS experimental flume [e.g., *Iverson*, 1997; *Iverson et al.*, 2010].

## 5. Conclusions

We experimentally created small-scale debris flows having self-formed levees and a marked depositional lobe, with flow behavior, deposit morphology, and sediment sorting that were similar to many natural debris flows. The width-to-depth ratio of small-scale experimental debris flows was in the range of natural debris flows. Debris flow runout was also in the range of natural debris flows, but flows were relatively short due to high friction.

Debris flow composition has a profound effect on depositional mechanism, runout, and deposit geometry in our experiments. Debris flow runout increases with an increase in channel slope and width, outflow plain slope, debris flow volume, and water fraction. There is an optimum debris flow composition for maximum runout. Increasing coarse-material fraction increases runout, probably by increased flow confinement by levee formation and grain collisional forces. However, too large coarse-material concentrations cause large frontal accumulations of coarse debris that reduce runout distance, probably by increasing frontal friction together with increased pore fluid pressure decay because of higher diffusivity. An increase in clay fraction enhances runout, most likely because of better retained excess pore pressures. However, too large proportions of clay (>0.22) make debris flows highly viscous so that runout is reduced. Deposition of clay-rich debris flows is likely mainly driven by viscosity and yield strength.

The geometry of debris flow deposits is strongly controlled by debris flow composition: the coarse-grained, clay, and water fractions all have a profound effect on lobe height, lobe width, and levee height. On the other hand, effects of initial conditions of topography (i.e., outflow plain slope, channel slope, and width) and volume are negligible in our experiments.

A loose erodible bed enabling infiltration was essential for the formation of well-developed self-formed levees and grain size segregation in our small-scale experiments. This may explain the absence of these features in previous small-scale experiments.

**Acknowledgments**

This work was supported by the Netherlands Organization for Scientific Research (NWO) and the Netherlands Space Office (NSO) (grant ALW-GO-PL17-2012 to M.G.K.). This work is part of the PhD research of T.d.H., MSc research of L.B., and BSc research of I.L. We gratefully acknowledge valuable discussions with Dario Ventra, Theo van Asch, and Henk van Steijn and technical support by Chris Roosendaal, Henk Markies, and Marcel van Maarseveen. Constructive reviews by James W. Vallance, Brian McArdell, Associate Editors Jon Major and Jason Kean, and one anonymous reviewer helped to improve the manuscript and are gratefully acknowledged. The authors contributed in the following proportions to conception and design, data collection, analysis and conclusions, and manuscript preparation: T.d.H. (60, 30, 50, and 70%), L.B. (0, 40, 20, and 10%), J.R.F.W.L. (10, 15, 0, and 0%), I.R.L. (0, 15, 10, and 0%), and M.G.K. (30, 0, 20, and 20%). Supplementary spreadsheet summarizes all data. DEMs are available for more detailed analysis upon request.

## References

Armanini, A., H. Capart, L. Fraccarollo, and M. Larcher (2005), Rheological stratification in experimental free-surface flows of granular-liquid mixtures, *J. Fluid Mech.*, *532*, 269–319.

Bagnold, R. A. (1954), Experiments on a gravity-free dispersion of large solid spheres in a Newtonian fluid under shear, *Proc. R. Soc. A*, *225*(1160), 49–63.

Bathurst, J., A. Burton, and T. Ward (1997), Debris flow run-out and landslide sediment delivery model tests, *J. Hydraul. Eng.*, *123*(5), 410–419.

Berti, M., and A. Simoni (2007), Prediction of debris flow inundation areas using empirical mobility relationships, *Geomorphology*, *90*(1), 144–161.

Bettella, F., T. Bisantino, V. D'Agostino, and F. Gentile (2012), Debris-flow runout distance: Laboratory experiments on the role of Bagnold, Savage and friction numbers, *WIT Trans. Eng. Sci.*, *4*, 27–36.

Blair, T. C. (1999), Sedimentology of the debris-flow-dominated Warm Spring Canyon alluvial fan, Death Valley, California, *Sedimentology*, *46*(5), 941–965, doi:10.1046/j.1365-3091.1999.00260.x.

Blair, T. C., and J. G. McPherson (1998), Recent debris-flow processes and resultant form and facies of the Dolomite alluvial fan, Owens Valley, California, *J. Sediment. Res.*, *68*(5), 800–818, doi:10.2110/jsr.68.800.

Bulmer, M. H., O. S. Barnouin-Jha, M. N. Peitersen, and M. Bourke (2002), An empirical approach to studying debris flows: Implications for planetary modeling studies, *J. Geophys. Res.*, *107*(E5), 1–16, doi:10.1029/2001JE001531.

Caine, N. (1980), The rainfall intensity: Duration control of shallow landslides and debris flows, *Geogr. Ann. A*, *62*(1–2), 23–27.

Cavalli, M., and L. Marchi (2008), Characterisation of the surface morphology of an alpine alluvial fan using airborne LiDAR, *Nat. Hazards Earth Syst. Sci.*, *8*(2), 323–333.

Corominas, J. (1996), The angle of reach as a mobility index for small and large landslides, *Can. Geotech. J.*, *33*(2), 260–271.

Costa, J. E. (1988), Rheologic, geomorphic, and sedimentologic differentiation of water flood, hyperconcentrated flows, and debris flows, in *Flood Geomorphology*, chap. Rheologic, geomorphic, and sedimentologic differentiation of water floods, hyperconcentrated flows, and debris flows, pp. 113–122, John Wiley, New York.

Coussot, P., and S. Proust (1996), Slow, unconfined spreading of a mudflow, *J. Geophys. Res.*, *101*(B11), 25,217–25,229.

Coussot, P., D. Laigle, M. Arattano, A. Deganutti, and L. Marchi (1998), Direct determination of rheological characteristics of debris flow, *J. Hydraul. Eng.*, *124*(8), 865–868.

Crosta, G., S. Cucchiaro, and P. Frattini (2003), Validation of semi-empirical relationships for the definition of debris-flow behavior in granular materials, in *3rd International Conference on Debris-Flow Hazards Mitigation*, pp. 821–831, Millpress Science Publ., Rotterdam, Netherlands.

D'Agostino, V., M. Cesca, and L. Marchi (2010), Field and laboratory investigations of runout distances of debris flows in the Dolomites (Eastern Italian Alps), *Geomorphology*, *115*(3), 294–304.

D'Agostino, V., F. Bettella, and M. Cesca (2013), Basal shear stress of debris flow in the runout phase, *Geomorphology*, *201*, 272–280.

Davies, T. R. H. (1990), Debris-flow surges: Experimental simulation, *J. Hydrol.*, *29*(1), 18–45.

De Ruig, J. H. M., and F. M. J. Hoozemans (1986), Debris flows in de Franse Alpen, Master's thesis, Universiteit Utrecht, Utrecht, Netherlands.

Fannin, R., and M. Wise (2001), An empirical-statistical model for debris flow travel distance, *Can. Geotech. J.*, *38*(5), 982–994.

George, D. L., and R. M. Iverson (2014), A depth-averaged debris-flow model that includes the effects of evolving dilatancy: II. Numerical predictions and experimental tests, *Proc. R. Soc. A*, *470*, 20,130,820, doi:10.1098/rspa.2013.0820.

Gray, J., and B. Kokelaar (2010), Large particle segregation, transport and accumulation in granular free-surface flows, *J. Fluid Mech.*, *652*, 105–137.

Griswold, J. P., and R. M. Iverson (2008), *Mobility Statistics and Automated Hazard Mapping for Debris Flows and Rock Avalanches, U.S. Geol. Surv. Sci. Invest. Rep., 2007–5276,* Reston, Va.

Hirano, M., and M. Iwamoto (1981), Measurement of debris flow and sediment-laden flow using a conveyor-belt flume in a laboratory, in *Proceedings International Symposium on Erosion and Sediment Transport in Pacific Rim Steeplands*, vol. 132, pp. 225–230, IAHS Pub, Washington, D. C.

Hoefling, R. (2004), High-speed 3D imaging by DMD technology, in *Machine Vision Applications in Industrial Inspection XII*, pp. 188–194, Int. Soc. for Optics and Photonics, San Jose, Calif.

Hübl, J., and H. Steinwendtner (2000), Estimation of rheological properties of viscous debris flow using a belt conveyor, *Phys. Chem. Earth Part B*, *25*(9), 751–755.

Hungr, O. (1995), A model for the runout analysis of rapid flow slides, debris flows, and avalanches, *Can. Geotech. J.*, *32*(4), 610–623.

Hürlimann, M., D. Rickenmann, and C. Graf (2003), Field and monitoring data of debris-flow events in the Swiss Alps, *Can. Geotech. J.*, *40*(1), 161–175.

Hürlimann, M., D. Rickenmann, V. Medina, and A. Bateman (2008), Evaluation of approaches to calculate debris-flow parameters for hazard assessment, *Eng. Geol.*, *102*(3), 152–163.

Hürlimann, M., B. W. McArdell, and C. Rickli (2015), Field and laboratory analysis of the runout characteristics of hillslope debris flows in Switzerland, *Geomorphology*, *232*, 20–32.

Hutchinson, J. (1986), A sliding-consolidation model for flow slides, *Can. Geotech. J.*, *23*(2), 115–126.

Iverson, R. M. (1997), The physics of debris flows, *Rev. Geophys.*, *35*(3), 245–296.

Iverson, R. M. (2003), *Debris Flow Mechanics and Mitigation Conference*, chap. The debris–flow rheology myth, pp. 303–314, Mills Press, Davos.

Iverson, R. M. (2015), Scaling and design of landslide and debris-flow experiments, *Geomorphology*, *244*, 9–20.

Iverson, R. M., and R. P. Denlinger (2001), Flow of variably fluidized granular masses across three-dimensional terrain: 1. Coulomb mixture theory, *J. Geophys. Res.*, *106*(B1), 537–552.

Iverson, R. M., and D. L. George (2014), A depth-averaged debris-flow model that includes the effects of evolving dilatancy: I. Physical basis, *Proc. R. Soc. A*, *470*(2170), 20130,819, doi:10.1098/rspa.2013.0819.

Iverson, R. M., and R. G. LaHusen (1989), Dynamic pore-pressure fluctuations in rapidly shearing granular materials, *Science*, *246*(4931), 796–799.

Iverson, R. M., S. P. Schilling, and J. W. Vallance (1998), Objective delineation of lahar-inundation hazard zones, *Geol. Soc. Am. Bull.*, *110*(8), 972–984.

Iverson, R. M., M. Logan, R. G. LaHusen, and M. Berti (2010), The perfect debris flow? Aggregated results from 28 large-scale experiments, *J. Geophys. Res.*, *115*, F03005, doi:10.1029/2009JF001514.

Jakob, M. (2005), Debris-flow hazard analysis, in *Debris-Flow Hazards and Related Phenomena*, pp. 411–443, Springer, Berlin.

Jakob, M., and P. Friele (2010), Frequency and magnitude of debris flows on Cheekye River, British Columbia, *Geomorphology*, *114*(3), 382–395.

Johnson, A., and J. Rodine (1984), *Slope Instability*, vol. 1984, chap. Debris flow, pp. 257–361, Wiley, Chichester, England.

Johnson, A. M. (1970), *Physical Processes in Geology: A Method for Interpretation of Natural Phenomena—Intrusions in Igneous Rocks, Fractures, and Folds, Flow of Debris and Ice*, Freeman, Cooper, San Francisco, Calif.

Johnson, C., B. Kokelaar, R. Iverson, M. Logan, R. LaHusen, and J. Gray (2012), Grain-size segregation and levee formation in geophysical mass flows, *J. Geophys. Res.*, *117*, F01032, doi:10.1029/2011JF002185.

Johnson, K., and N. Sitar (1990), Hydrologic conditions leading to debris-flow initiation, *Can. Geotech. J.*, *27*(6), 789–801.

Kaitna, R., and D. Rickenmann (2007), Flow of different material mixtures in a rotating drum, in *Debris-Flow Hazards Mitigation, Fourth International DFHM Conference: Mechanics, Prediction and Assessment*, pp. 10–13, Millpress, Netherlands.

Kaitna, R., D. Rickenmann, and M. Schatzmann (2007), Experimental study on rheologic behaviour of debris flow material, *Acta Geotech.*, *2*(2), 71–85.

Klute, A., and C. Dirksen (2003), Hydraulic conductivity and diffusivity: Laboratory methods, in *Methods of Soil Analysis, Soil Science Society Of America Book Series*, Part 1, 687–734, Am. Soc. of Agronomy, Madison, Wis.

Larcher, M., L. Fraccarollo, A. Armanini, and H. Capart (2007), Set of measurement data from flume experiments on steady uniform debris flows, *J. Hydraul. Res.*, *45*(sup1), 59–71.

Liu, X. (1996), Size of a debris flow deposition: Model experiment approach, *Environ. Geol.*, *28*(2), 70–77.

Lowe, D. R. (1976), Grain flow and grain flow deposits, *J. Sediment. Res.*, *46*(1), 188–199.

Major, J. J. (1997), Depositional processes in large-scale debris-flow experiments, *J. Geol.*, *105*(3), 345–366.

Major, J. J. (2000), Gravity-driven consolidation of granular slurries—Implications for debris-flow deposition and deposit characteristics, *J. Sediment. Res.*, *70*(1), 64–83.

Major, J. J., and R. M. Iverson (1999), Debris-flow deposition: Effects of pore-fluid pressure and friction concentrated at flow margins, *Geol. Soc. Am. Bull.*, *111*(10), 1424–1434.
Marchi, L., and P. R. Tecca (2013), *Dating Torrential Processes on Fans and Cones*, chap. Debris–flow monitoring in Italy, pp. 309–318, Springer, Netherlands.
McCoy, S. W., J. W. Kean, J. A. Coe, D. M. Staley, T. A. Wasklewicz, and G. E. Tucker (2010), Evolution of a natural debris flow: In situ measurements of flow dynamics, video imagery, and terrestrial laser scanning, *Geology*, *38*(8), 735–738.
Parsons, J. D., K. X. Whipple, and A. Simoni (2001), Experimental study of the grain-flow, fluid-mud transition in debris flows, *J. Geology*, *109*(4), 427–447.
Pierson, T. C. (1984), Why debris flows stop, *GSA Abstracts with Programs*, *16*, 623.
Pierson, T. C. (1986), Flow behavior of channelized debris flows, Mount St. Helens, Washington, in *Hillslope Processes*, edited by A. D. Abrahams, pp. 269–296, Allen and Unwin, Boston.
Pierson, T. C. (2005), *Distinguishing Between Debris Flows and Floods From Field Evidence in Small Watersheds*, US Dep. of the Int., U.S. Geol. Survey, Reston, Va.
Prochaska, A. B., P. M. Santi, J. D. Higgins, and S. H. Cannon (2008), Debris-flow runout predictions based on the Average Channel Slope (ACS), *Eng. Geol.*, *98*(1), 29–40.
Rebetez, M., R. Lugon, and P. -A. Baeriswyl (1997), Climatic change and debris flows in high mountain regions: The case study of the Ritigraben torrent (Swiss Alps), *Clim. change*, *36*(3-4), 371–389.
Rickenmann, D. (1999), Empirical relationships for debris flows, *Nat. Hazards*, *19*(1), 47–77.
Rickenmann, D. (2005), *Debris-Flow Hazards and Related Phenomena*, chap. Runout Prediction Methods, pp. 305–324, Praxis, Chichester, U. K.
Savage, S., and R. Iverson (2003), *Debris Flow Mechanics and Mitigation Conference*, vol. 1, chap. Surge dynamics coupled to pore–pressure evolution in debris flows, pp. 503–514, Mills Press, Davos.
Savage, S. B., and K. Hutter (1989), The motion of a finite mass of granular material down a rough incline, *J. Fluid Mech.*, *199*, 177–215.
Scheidl, C., and D. Rickenmann (2010), Empirical prediction of debris-flow mobility and deposition on fans, *Earth Surf. Process. Landforms*, *35*(2), 157–173.
Scheidl, C., D. Rickenmann, and B. W. McArdell (2013), *Landslide Science and Practice*, chap. Runout Prediction of Debris Flows and Similar Mass Movements, pp. 221–229, Springer, Berlin.
Stoffel, M., T. Mendlik, M. Schneuwly-Bollschweiler, and A. Gobiet (2014), Possible impacts of climate change on debris-flow activity in the Swiss Alps, *Clim. Change*, *122*(1–2), 141–155.
Takahashi, T. (1978), Mechanical aspects of debris flow, *J. Hydraul. Div.*, *104*, 1153–1169.
Takahashi, T. (1991), *Debris Flow*, Balkema, Rotterdam, Netherlands.
Takahashi, T. (2009), A review of Japanese debris flow research, *Int. J. Erosion Control Eng.*, *2*(1), 1–14.
Tang, C., J. Zhu, M. Chang, J. Ding, and X. Qi (2012), An empirical–statistical model for predicting debris-flow runout zones in the Wenchuan earthquake area, *Quat. Inter.*, *250*, 63–73.
Terzaghi, K. (1956), Varieties of submarine slope failures, in *Proceedings of Eighth Texas Conference on Soil Mechanics and Foundation Engineering: Austin, University of Texas, Bureau of Engineering Research, Spec. Publ. 29*, Harvard Univ., Cambridge, Mass., 14–15 Sept.
Thomas, D. G. (1965), Transport characteristics of suspension: VIII. A note on the viscosity of Newtonian suspensions of uniform spherical particles, *J. Colloid Sci.*, *20*(3), 267–277.
Toyos, G., D. O. Dorta, C. Oppenheimer, M. T. Pareschi, R. Sulpizio, and G. Zanchetta (2007), GIS-assisted modelling for debris flow hazard assessment based on the events of May 1998 in the area of Sarno, Southern Italy: Part I. Maximum run-out, *Earth Surf. Processes Landforms*, *32*(10), 1491–1502, doi:10.1002/esp.1472.
Vallance, J. W., and S. B. Savage (2000), Particle segregation in granular flows down chutes, in *IUTAM Symposium on Segregation in Granular Flows*, pp. 31–51, Springer, Netherlands.
Van Steijn, H., and J. Coutard (1989), Laboratory experiments with small debris flows: Physical properties related to sedimentary characteristics, *Earth Surf. Processes Landforms*, *14*(6), 587–596.
Vanoni, V. A. (1975), *Sedimentation Engineering*, Am. Soc. of Civil Eng., New York.
Whipple, K. X., and T. Dunne (1992), The influence of debris-flow rheology on fan morphology, Owens Valley, California, *Geol. Soc. Am. Bull.*, *104*(7), 887–900.
Zanuttigh, B., and A. Lamberti (2007), Instability and surge development in debris flows, *Rev. Geophys.*, *45*, RG3006, doi:10.1029/2005RG000175.
Zhou, G. G., and C. W. Ng (2010), Dimensional analysis of natural debris flows, *Can. Geotech. J.*, *47*(7), 719–729.